NOTE FROM THE EDITOR

ARCHIVES of ACOUSTICS is an English version of the quarterly ARCHIWUM AKUSTYKI which has been published in Polish since 1966, apart from a few papers appeared in other foreign languages, only the summaries of individual papers and the figure captions being printed in English.

However, the development of the cooperation of Polish acoustical centers with the foreign ones has evoked an increasing interest in the Polish periodical abroad. For this reason the publication of ARCHIVES of ACOUSTICS as a correlated version of ARCHIWUM AKUSTYKI for foreign readers was decided upon.

The new English edition of the acoustical periodical follows from the universal tendency towards the development of acoustics which is a wide and complex discipline, comprising different branches of knowledge. Both the increase of acoustical societies and organizations in the world and the increasing number of general or specialized conferences, as well as the increasing number of their participants confirm this intensive development. As a result, the amount of material for print is growing; it is hoped that the publication of the papers of foreign authors in ARCHIVES of ACOUSTICS will help to meet the growing demand for print.

The Editorial Committee of ARCHIVES of ACOUSTICS accept only original, both theoretical and experimental papers on acoustics, not previously published, which may be of interest to scientific and practical purposes. Moreover, short technical reviews in the field of acoustics, Letters to the Editor and short reports concerning the most important congresses and meetings will be published.

The quarterly will also disseminate information on the scientific and technical activities of Polish and foreign societies and research centers dealing with acoustics.

ARCHIVES of ACOUSTICS will appear quarterly simultaneously with ARCHIWUM AKUSTYKI. The content of the English version will be about 25 % less than that of the Polish one since some articles and information published in ARCHIWUM AKUSTYKI may have only local importance, being of no interest to foreign readers.

In presenting the first issue of ARCHIVES of ACOUSTICS the Editor hopes that this issue and future ones will evoke the Readers' interest and will stimulate the cooperation of Polish and foreign acousticians. Contributions both from Poland and abroad are welcome.

The Editor would be very happy to have an opportunity of cooperation with other periodicals on acoustics.

Editor-in-Chief

Prof. Stefan Czarnecki, Ph.D.

ARCHIVES OF ACOUSTICS
1, 1, 5-19 (1976)

NOISE SOURCES IDENTIFICATION IN MACHINES AND MECHANICAL DEVICES

CZESŁAW CEMPEL, URSZULA KOSIEL

Technical University (Poznań)

This paper presents a method for the determination of noise sources locations in machines and mechanical devices. It also describes a method for the determination of the nature of these noise sources and their effect on the overall noise. The former is based on the properties of the frequency band correlation function, the latter on the properties of the coherence function. It is shown that these two methods can be used in attempts to minimize machine noise.

1. Introduction

Most modern machines in use and manufactured today are characterized by vibro-acoustical energy of large magnitudes and by complexity. The vibro-acoustical output depends on how much of the supplied driving energy is converted into dynamic disturbances which produce vibration and noise.

These dynamic disturbances are harmful to man and the environment as well as to the machine itself since they cause material fatigue which decreases durability and reliability. The best method of reducing these undesired effects is to decrease the disturbances at their sources. However, the construction and performance of modern machines is often so complicated that, in many cases, it is difficult to determine the exact location of the disturbance sources and their physical nature without special measurements. The present work offers one method for determining the location of noise sources in machines and mechanical devices and another method for the determination of their characteristics. In other words, the method described here should make it possible to determine where the noise is produced and what its nature is, with respect to the classification of noises as either mechanical or aerodynamical.

2. The relations between vibro-acoustical processes in machines

By *vibro-acoustical processes*, we mean the noise or vibration produced by machines. These processes can be measured using suitable transducers at the following locations: in the surroundings of the machine, at the machine parts or inside the working space of the machine (e.g. in a combustion chamber).

It is obvious that most vibro-acoustical processes in machines as measured at these points will have something in common. This similarity can be divided into two classes: the general one — when the processes occur in the same machine, and the particular one — when the processes have the same source in the machine. The theory of stationary ergodic random processes, including vibro-acoustical ones, distinguishes two measures of similarity between them, namely the correlation function and the coherence function [1]. With regard to the manner in which the correlation function is calculated it can be recognized as a measure of the general similarity of the processes in the time domain and determines the similarity of two processes within a definite time interval. On the other hand, the coherence function determines the maximum similarity of processes in terms of the frequency spectrum. It does not contain any phase information (for the following procedures, phase information is not necessary). For multi-resonant systems in machines and their elements, coherence functions are much easier to interprete than correlation functions [2]. Hence, the coherence function is a measure of the detailed similarity between the processes and makes it possible to distinguish between the separate disturbance sources in the machine.

These two measures of similarity between the processes are interrelated by the normalized correlation measured over the frequency band. Therefore, we begin with determining the correlation function.

Let the two vibro-acoustical processes have the forms $x_1(t)$ and $y_1(t)$, measured either in the machine or in its surroundings. The correlation function of these processes $\psi_{x_1y_1}(\tau)$ can be expressed by means of the cross-power spectral density $W_{x_1y_1}(f)$ through the Wiener-Khinchin [1] relation

$$\psi_{x_1y_1}(\tau) = \int_{-\infty}^{\infty} W_{x_1y_1}(f) e^{j2\pi f\tau} df, \tag{1}$$

where f is frequency, τ — the time delay between the two processes and j — the imaginary unit.

The cross-spectral density $W_{x_1y_1}(f)$ is a complex quantity and, thus it can be expressed in the form $W_{x_1y_1}(f) = |W_{x_1y_1}(f)| e^{-j\varphi}$. The phase shift $\varphi = \varphi(f)$ depends on the frequency and shows the relationship between the real and imaginary components of the spectral density.

Since the correlation function is a real quantity, it follows from (1) that

$$\psi_{x_1y_1}(\tau) = \int_{-\infty}^{\infty} |W_{x_1y_1}(f)| e^{j(2\pi f\tau - \varphi)} df = 2\int_{0}^{\infty} |W_{x_1y_1}(f)| \cos(2\pi f\tau - \varphi) df. \tag{2}$$

It is well known that it is possible to derive from (2) a normalized correlation function making use of the expressions

$$\varrho_{x_1y_1}(\tau) = \frac{\psi_{x_1y_1}(\tau)}{\sqrt{\sigma_{x_1}^2 \sigma_{y_1}^2}},$$

$$\sigma_{x_1}^2 = 2\int_0^\infty W_{x_1x_1}(f)\,df, \qquad \sigma_{y_1}^2 = 2\int_0^\infty W_{y_1y_1}(f)\,df, \tag{3}$$

where $\sigma_{x_1}^2$ and $\sigma_{y_1}^2$ denote the variances of the processes $x_1(t)$ and $y_1(t)$.

Thus, from (2) and (3) the normalized correlation function of the two processes is expressed by

$$\varrho_{x_1y_1}(\tau) = \frac{\int_0^\infty |W_{x_1y_1}(f)|\cos(2\pi f\tau - \varphi)\,df}{\sqrt{\int_0^\infty W_{x_1x_1}(f)\,df \int_0^\infty W_{y_1y_1}(f)\,df}}. \tag{4}$$

It is known that the normalized correlation function of Gaussian processes can most conveniently be measured by means of the polar correlator [4]. Let the processes $x_1(t)$ and $y_1(t)$ from the vibro-acoustical field of the machine be

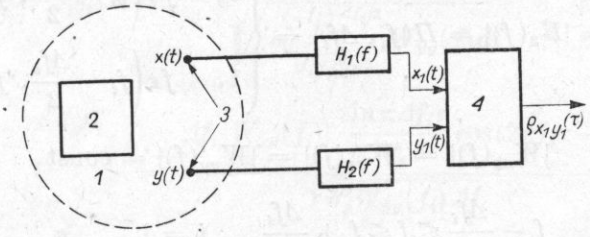

Fig. 1. General schematic representation of measurement procedure
1 – vibro-acoustical field, *2* – machine or mechanical device under test, *3* – transducers, *4* – polar correlator

fed to the input of the correlator. Let the transmittance of the measuring channels $x(t)$ and $y(t)$, be $H_1(f)$ and $H_2(f)$ respectively as shown in Fig. 1. From the diagram of signal transmission shown in Fig. 1, the spectral relations in (4) between the processes $x_1(t)$, $y_1(t)$, $x(t)$ and $y(t)$ can be expressed [5] by

$$\begin{gathered} W_{x_1x_1}(f) = |H_1(f)|^2 W_{xx}(f), \qquad W_{y_1y_1}(f) = |H_2(f)|^2 W_{yy}(f), \\ W_{x_1y_1}(f) = H_1(f)H_2^*(f)W_{xy}(f), \end{gathered} \tag{5}$$

where $W_{xx}(f)$ and $W_{yy}(f)$ denote the power spectral densities of the processes $x(t)$ and $y(t)$ respectively, and $W_{xy}(f)$ the cross-spectral density of the vibro-acoustical processes $x(t)$ and $y(t)$ (the asterisk denotes a conjugate complex). Substituting the spectral relations (5) into (4) yields

$$\varrho_{x_1y_1}(\tau) = \frac{\int_0^\infty |W_{xy}(f)H_1(f)H_2^*(f)|\cos(2\pi f\tau - \varphi)\,df}{\int_0^\infty W_{xx}(f)|H_1(f)|^2\,df \int_0^\infty W_{yy}(f)|H_2(f)|^2\,df}. \tag{6}$$

Thus by introducing the spectral transmittances of the measuring channels the relations between the normalized correlation function and the spectral properties of the processes measured can be derived.

The formula (6) will now be used for the determination of the spectral-correlation method for the investigation of vibro-acoustical processes.

3. The spectral-correlation method

Let us assume initially that the transmittances of the measuring channels can be represented by identical band-pass filters with mid-frequency f_i which have a flat transmission curve over their bandwidth. Let us further assume that the spectral densities of the processes of interest here are smooth functions also flat in the transmittance band Δf_i. Hence we can write

$$|H_1(f)| = |H_2(f)| = \Pi(f_i, \Delta f_i) = \begin{cases} 0, & f \notin \left(f_i - \dfrac{\Delta f_i}{2}, f_i + \dfrac{\Delta f_i}{2}\right), \\ 1, & f \in \left(f_i - \dfrac{\Delta f_i}{2}, f_i + \dfrac{\Delta f_i}{2}\right), \end{cases} \tag{7}$$

$$|W_{xy}(f)| = |W_{xx}(f)| = |W_{yy}(f)| = \text{const},$$

$$f_i - \frac{\Delta f_i}{2} \leqslant f \leqslant f_i + \frac{\Delta f_i}{2}, \quad i = 1, \ldots, n.$$

We insert the above formulae into (6) and perform transformations to obtain

$$\varrho_{x_1 y_1}(\tau) = \frac{\int\limits_{f_i - \Delta f_i/2}^{f_i + \Delta f_i/2} |W_{xy}(f)| \cos(2\pi f\tau - \varphi)\, df}{\sqrt{\int\limits_{f_i - \Delta f_i/2}^{f_i + \Delta f_i/2} W_{xx}(f)\, df \int\limits_{f_i - \Delta f_i/2}^{f_i + \Delta f_i/2} W_{yy}(f)\, df}} \tag{8}$$

$$= \frac{|W_{xy}(f_i)| \dfrac{\sin \pi \Delta f_i \tau}{\pi \Delta f_i \tau} \cos(2\pi f_i \tau - \varphi)}{\sqrt{W_{xx}(f_i) W_{yy}(f_i)}}.$$

It is well known [1, 2, 3] that the coherence function of two random processes is expressed as follows

$$\gamma_{xy}^2(f) = \frac{|W_{xy}(f)|^2}{W_{xx}(f) W_{yy}(f)}. \tag{9}$$

Hence, the normalized correlation function within the band Δf_i, (8) can be written in the following form:

$$\varrho_{x_1y_1}(\tau) = \gamma_{xy}(f_i)\frac{\sin \pi \Delta f_i \tau}{\pi \Delta f_i \tau}\cos(2\pi f_i \tau - \varphi), \qquad \varphi = \varphi(f_i). \tag{10}$$

Thus we have obtained the relation between the spectral similarity measure of processes $\gamma^2_{xy}(f_i)$ and the normalized band correlation function of those processes. The question of how to use this relation in practice will be dealt with later.

We shall now consider another possible form of the transmittance of measuring channels (Fig. 1).

Let us now assume that the transmittance of a measuring channel of the process $x(t)$ has unit gain (i.e. $|H_1(f)| = 1$), while the transmittance of the second channel $H_2(f)$ and the spectral densities satisfy equation (7). On the basis of these assumptions and (6) we can write

$$\varrho_{x_1y_1}(\tau) = r_{x_1y_1}(\tau) = \frac{\int\limits_{f_i-\Delta f_i/2}^{f_i+\Delta f_i/2} |W_{xy}(f)|\cos(2\pi f\tau - \varphi)\,df}{\sqrt{\sigma_x^2 \int\limits_{f_i-\Delta f_i/2}^{f_i+\Delta f_i/2} W_{yy}(f)\,df}}$$

$$= \frac{\Delta f_i |W_{xy}(f_i)| \dfrac{\sin \pi \Delta f_i \tau}{\pi \Delta f_i \tau}\cos(2\pi f_i \tau - \varphi)}{\sqrt{\sigma_x^2 W_{yy}(f_i)\,\Delta f_i}}. \tag{11}$$

To make expressions (10) and (11) similar, let us transform the factor linked with the trigonometric expressions

$$\frac{\Delta f_i |W_{xy}(f_i)|}{\sqrt{\sigma_x^2 W_{yy}(f_i)\,\Delta f_i}} = \sqrt{\frac{(\Delta f_i)^2 |W_{xy}(f_i)|^2}{\sigma_x^2 W_{yy}(f_i)\,\Delta f_i}}$$

$$= \sqrt{\frac{\Delta f_i W_{xx}(f_i)\,|W_{xy}(f_i)|^2}{\sigma_x^2 W_{xx}(f_i) W_{yy}(f_i)}} = \sqrt{E_x^2(f_i)\gamma_{xy}^2(f_i)}, \tag{12}$$

where $E_x^2(f_i) = \Delta f_i W_{xx}(f_i)/\sigma_x^2$.

Apart from the coherence of processes (9) we have introduced here a new quantity $E_x^2(f_i)$ which can be termed the energy contribution of the band Δf_i of the process $x(t)$ to the total energy of the whole process, because

$$E_x^2(f_i) = \frac{\text{variance in band } \Delta f_i}{\text{total variance}} = \frac{\Delta f_i W_{xx}(f_i)}{\sigma_x^2}. \tag{13}$$

Hence it follows that the normalized band correlation function of the processes $x(t)$ and $y(t)$, as measured using one filter, takes the final form

$$r_{x_1y_1}(\tau) = E_x(f_i)\gamma_{xy}(f_i)\frac{\sin \pi \Delta f_i \tau}{\pi \Delta f_i \tau}\cos(2\pi f_i \tau - \varphi). \tag{14}$$

Comparing the final expressions (10) and (14), we can easily find that they are similar in character, i.e. the terms depending on the time delay τ between the processes are identical while terms depending on the spectral pattern of the processes under discussion are analogous.

Let us notice now that, on the basis of properties of the function $(\sin x)/x$ and the experimental results [6], it is possible to simplify these expressions because

$$\frac{\sin \pi \Delta f_i \tau}{\pi \Delta f_i \tau} \approx 1, \quad \Delta f_i \tau \leqslant 0.2. \tag{15}$$

Then, with equation (15) satisfied, we have

$$\varrho_{x_1 y_1}(\tau) = \gamma_{xy}(f_i) \cos(2\pi f_i \tau - \varphi) \tag{16}$$

and

$$r_{x_1 y_1}(\tau) = E_x(f_i) \gamma_{xy}(f_i) \cos(2\pi f_i \tau - \varphi). \tag{17}$$

If we now find the values of the two functions for such time instants τ_0, τ_1 that $\tau_1 = \tau_0 + 1/4f_i$ (for which there is a corresponding phase shift $\pi/2$ at the frequency f_i, easily obtained by electrical means) and that according to (15)

$$\Delta f_i \left(\tau_0 + \frac{1}{4f_i}\right) < 0.2,$$

then the sum of squares of these functions yields

$$\gamma_{xy}^2(f_i) = [\varrho_{x_1 y_1}(\tau_0)]^2 + [\varrho_{x_1 y_1}(\tau_1)]^2, \tag{18}$$

$$E_x^2(f_i) \gamma_{xy}^2(f_i) = [r_{x_1 y_1}(\tau_0)]^2 + [r_{x_1 y_1}(\tau_1)]^2. \tag{19}$$

It follows that by the measurement of the polar correlation function using two identical filters, it is possible to determine the coherence function of processes, whereas using only one filter the product of a coherence function and the energy contribution of unfiltered process can be determined. The energy contribution of the process $x(t)$ can be easily determined by means of the same filter, so if $E_x^2(f_i) \neq 0$, the two methods can be recognized as equivalent.

It is obvious that the use of a single filter is simpler from the point of view of the measuring equipment, whereas the method of two filters is faster.

Knowing the coherence function of a process within a frequency band f_i, it is possible to determine directly a measure of the statistical similarity or identity of these processes, since $\gamma_{xy}^2(f_i) = 1$ denotes the processes statistically identical over the frequency band under consideration, $0 < \gamma_{xy}^2(f_i) < 1$ denotes the processes only statistically similar over the frequency band under consideration, and $\gamma_{xy}^2(f_i) = 0$ denotes the processes statistically different over the frequency band under consideration. Thus the coherence function indicates the degree of dependence between vibro-acoustic processes, their origin, and the relative significance of a given partial process in complex processes etc.

4. The identification of noise sources

The spectral correlation method presented here can, in general, be employed for determining the source location of both vibration and noise in machines. However for vibration it is required that additional assumptions concerning the resonance and dissipation properties of the machine investigated are satisfied. Therefore, the discussion here is limited to the determination of the location of noise source and its nature in machines and devices.

An analysis of formulae (16) and (17) shows that to determine the location of a partial noise source in a machine two procedures can be used. In the first procedure the measure of similarity between the partial noise source and the resultant noise in the machine is used. This can be done if the coherence function is known. Let us assume that the process $x(t)$ represents the resultant overall

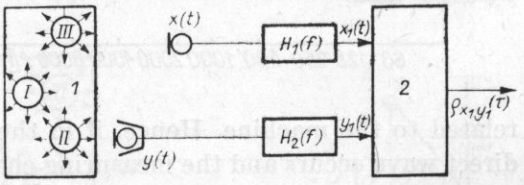

Fig. 2. Schematic representation of coherence measurement procedure
1 – machine or mechanical device, *2* – polar correlator

noise of the machine measured sufficiently far from it, while the process $y(t)$ is the partial noise measured at a very close range from its source. The measurement set-up is shown in Fig. 2 where Roman numerals denote the presupposed locations of the noise sources.

By performing the measurements according to formulae (16) and (17) we shall find the value of coherence within each frequency band of the process analyzed. Plotting these values as a function of frequency for each of the sources, we can find the two extreme forms of the coherence function.

A flat form and a low value of coherence indicates that the partial noise sources are equally significant with respect to the chosen measuring point for the channel $y(t)$.

A coherence function with one or several maxima indicates that a significant partial noise source in a given band (the corresponding curves *1* and *2* in Fig. 3) is close to the measuring point.

Thus, a method of trial and error, in which many microphone locations for the partial noise sources are employed, will determine the location of the important noise sources and their relative significance.

The second procedure used for the determination of noise source locations follows from the directional properties of (16) and (17) and is based on the change of time delay from changes of positions of the transducers. This procedure is similar to that proposed by GOFF [7] but, in this case, the object of measurement is the frequency band correlation function.

Let us assume that two microphones are mounted on a rotary arm at a

distance d as shown in Fig. 4. Assuming plane waves and rotation of the arm by an angle α, the difference in distance between the microphones is $l = d\sin\alpha$. The time delay related to this difference is $\tau = (d\sin\alpha)/c$, where c is the sound velocity in air. Fig. 4 shows that the processes $x(t)$ and $y(t)$ are identical as

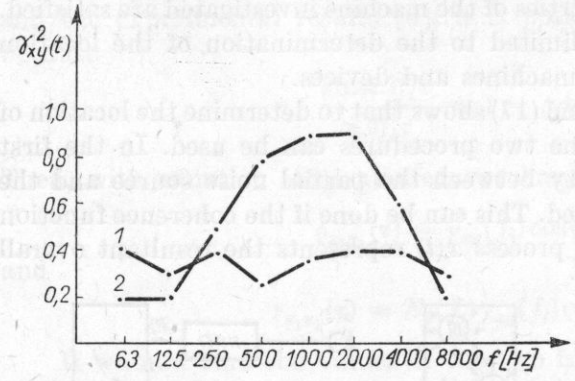

Fig. 3. Coherence of different sources
1 – no-determining of sound source location,
2 – determining of sound source location

related to the machine. Hence, if in the measuring room only the field of the direct wave occurs and the measuring channels are identical, we can assume that

$$\gamma_{xy}(f_i) \simeq 1, \quad \varphi(f_i) \simeq 0.$$

Thus formulae (16) and (17) are simplified to the form

$$\begin{aligned} \varrho_{x_1y_1}(\tau) &\cong \cos\left(\frac{2\pi f_i d\sin\alpha}{c}\right), \\ r_{x_1y_1}(\tau) &\cong E_x(f_i)\cos\left(\frac{2\pi f_i d\sin\alpha}{c}\right). \end{aligned} \tag{20}$$

It is clear that by looking for the maxima of functions (20) through the change of angle α, the direction of an arbitrary noise source in a given frequency band Δf_i can be found.

Let us return now to the relation which restricts the time change τ (15). By substituting the time resulting from the change of the distance l into (15) we obtain

$$\Delta f_i \tau = \Delta f_i \frac{|d\sin\alpha|}{c} \leqslant 0.2. \tag{21}$$

Most investigations of vibro-acoustical processes, particularly noise, are carried out by means of filters with a constant relative bandwidth β, $\beta = \Delta f_i/f_i = \text{const}$, where for octave filters $\beta = 0.7071$, for $\frac{1}{3}$ octave filters $\beta = 0.2310$.

Taking it into consideration in (21), we get

$$\frac{\Delta f_i |d\sin\alpha|}{c} = \frac{\beta f_i |d\sin\alpha|}{c} = \frac{\beta |d\sin\alpha|}{\lambda_i} \leqslant 0.2, \tag{22}$$

where $\lambda_i = c/f_i$ is an acoustical wave length corresponding to a frequency f_i. Restricting α to the desired scanning angle $\alpha = \pm 15°$ we obtain

$$\frac{d}{4\lambda_i} \leqslant \frac{0.2}{\beta}. \tag{23}$$

Hence, the distances between microphones and the wavelengths for particular filters should satisfy the relations:

$$\begin{aligned} d/\lambda_i &\leqslant 1 \quad \text{for octave filters,} \\ d/\lambda_i &\leqslant 4 \quad \text{for } \tfrac{1}{3}\text{-octave filters.} \end{aligned} \tag{24}$$

Now, by positioning the machine in such a way that its angular width does not exceed 30° and restrictions (24) are satisfied, it is possible to find the location of the main noise sources for each band Δf_i. Similar restrictions are imposed

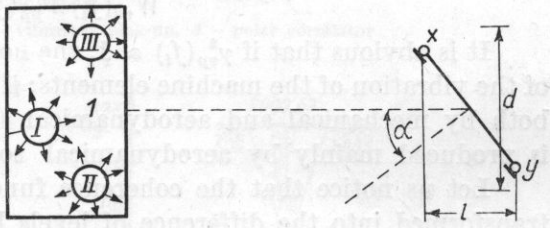

Fig. 4. Schematic representation of measurement procedure for the determination of locations of the noise sources
1 – machine or mechanical device

on the method of coherence using formulae (18) and (19). The required time delay $\Delta\tau = \tau_0 - \tau_1 = 1/(4f_i)$ must satisfy the same relation, that is $\Delta f_i \Delta\tau \leqslant 0.2$. By expressing Δf_i in terms of the relative bandwidth $\Delta f_i = \beta f_i$, we obtain the condition

$$\frac{\beta}{4} \leqslant 0.2, \quad \text{i.e.} \quad \beta \leqslant 0.8. \tag{24a}$$

It follows that inequality (24a) for octave filters $\beta = 0.7071$ is still satisfied. Therefore with all the remaining conditions being satisfied, these filters may be utilized for determining the coherence function as well.

When the locations of the sources of noise have been found, it may be possible to determine where the noise is generated, and to what degree and in which frequency bands the noise is produced by vibration of machine parts or by turbulent flow of the medium. Thus it becomes necessary to use, once more, the properties of the coherence function by placing the microphone $x(t)$ at the point $y(t)$ as shown in Fig. 2. Let the process $y(t)$ be the velocity of vibration of a machine element in the neighbourhood of the source under investigation. The noise received by the microphone is denoted by $p(t)$, $[x(t) \rightarrow p(t)]$ and the velocity of vibration of the machine element by $v(t)$, $[y(t) \rightarrow v(t)]$.

The noise $p(t)$ is the non-correlated sum of the mechanical noise $m(t)$ and the aerodynamic noise $n(t)$, so that

$$x(t) = p(t) = m(t)+n(t),$$
$$W_{pp}(f) = W_{mm}(f)+W_{nn}(f). \tag{25}$$

Assume also that the transmittance of vibration velocity into mechanical noise is denoted by the transfer function $H(f)$. Then, $W_{mm}(f) = |H(f)|^2 W_{vv}(f)$. It can be shown that with no correlation between the vibration velocity and aerodynamic noise, the following relationship is valid:

$$|W_{vp}(f)|^2 = W_{vv}^2(f)|H(f)|^2 = W_{vv}(f)W_{mm}(f). \tag{26}$$

Thus the value of coherence between the vibration velocity and noise at the point considered for the Δf_i band can be expressed in the following form:

$$\gamma_{vp}^2(f_i) = \frac{|W_{vp}(f_i)|^2}{W_{vv}(f_i)W_{pp}(f_i)} \cong \frac{W_{mm}(f_i)}{W_{pp}(f_i)}. \tag{27}$$

It is obvious that if $\gamma_{vp}^2(f_i) \approx 1$, the noise is mainly the result of conversion of the vibration of the machine elements; if $0 < \gamma_{vp}^2(f_i) < 1$ the noise is produced both by mechanical and aerodynamical sources and if $\gamma_{vp}^2(f_i) \approx 0$, the noise is produced mainly by aerodynamical sources.

Let us notice that the coherence function (27) can, in a simple way, be transformed into the difference of levels between the resultant noise L_p and the noise produced by mechanical sources L_m. By expressing (27) in terms of the noise levels, we get

$$\Delta L_{pm_i} = L_{p_i} - L_{mi} = 10\log\frac{1}{|\gamma_{vp}(f_i)|^2}, \tag{28}$$
$$|\gamma_{vp}(f_i)| < 1.$$

A similar transformation can be applied to the energy contribution $E_p^2(f_i)$ in formula (17).

It is known that, if the level difference from two sources exceeds 10 dB, the effect of the source with a lower level on the resultant noise is negligible. This fact taken into account in formula (28) shows that for $|\gamma_{vp}(f_i)| < 0{,}3$ the effect of vibration on the noise level of the source is insignificant. It follows from this reasoning that the measured coherences of vibration, velocity and noise of a given source can show how this noise is generated and what is the significance of the mechanical component with regard to the resultant noise level.

Summarizing the discussion so far it can be stated that with the use of instruments functioning as defined by the formulae (16) to (19), it is possible to determine the locations of noise sources in the machine and the means by which the noise is generated. Moreover, this informations is obtainable for each separate frequency band.

5. Experimental investigations

To estimate the usefulness of the method described for the vibro-acoustical investigation of machines and mechanical devices, we prepared a laboratory experiment. A block diagram of the measuring apparatus is shown in Fig. 5.

It consisted of two equivalent channels, each containing the MPDA-10 noise level meter with an analyzer to measure the noise and vibration in the octave bands from 63 Hz to 8 kHz.

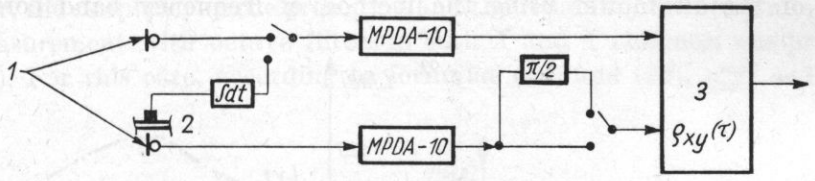

Fig. 5. Experimental set-up for the identification of noise and vibration sources in machines

1 – condenser microphones, *2* – vibration pick-up, *3* – polar correlator

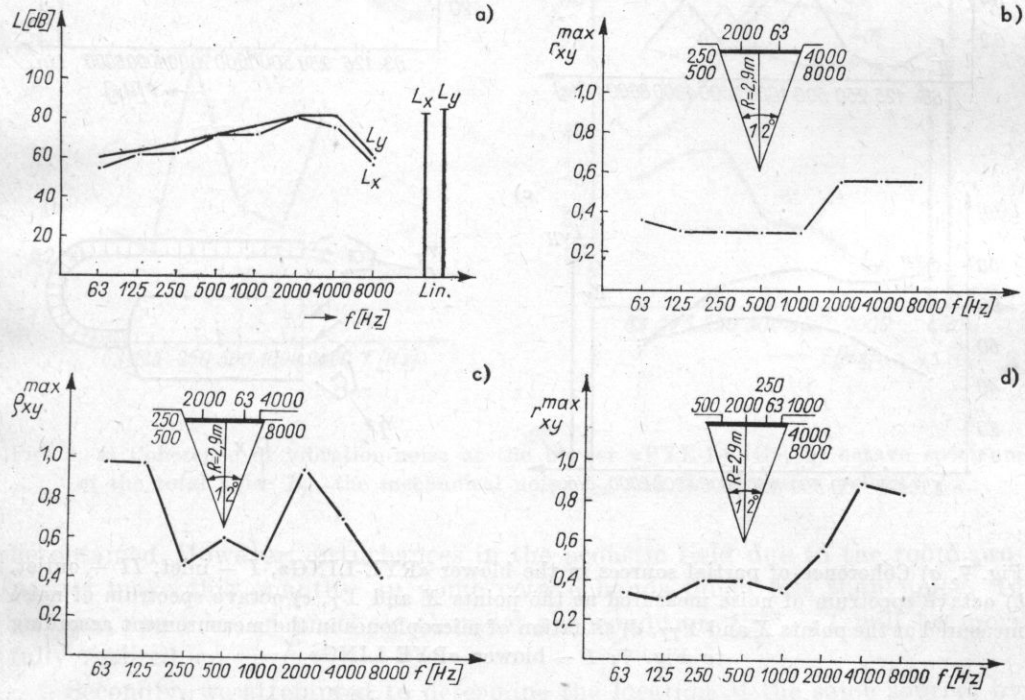

Fig. 6. *a*) Octave spectrum of noise measured at the points X and Y, *b*) results of the determination of the noise source locations in the blower «PYE-LING» – using $r_{xy}^{\max}$, *c*) results of the determination of the noise source locations in the blower «PYE-LING» – using $\varrho_{xy}^{\max}$, *d*) results of the determination of the noise source locations in the blower «PYE-LING» – using $r_{xy}^{\max}$

Output voltages from the two channels were fed to a polar correlator (designed by the authors of this report) directly or through a phase shifter $\varphi = 90°$ in one of the channels. This set-up was used for investigating two noise sources, namely a «PYE-LING» blower designed for air cooling of vibration exciter units and also a one-cylinder portable compressor. The experiments were performed in a laboratory room about $11 \times 5 \times 3$ m^3, in which it was impossible to measure only the direct waves generated by the source.

Firstly, we performed experiments to determine the location of the noise sources of the air blower using the method of frequency band correlation.

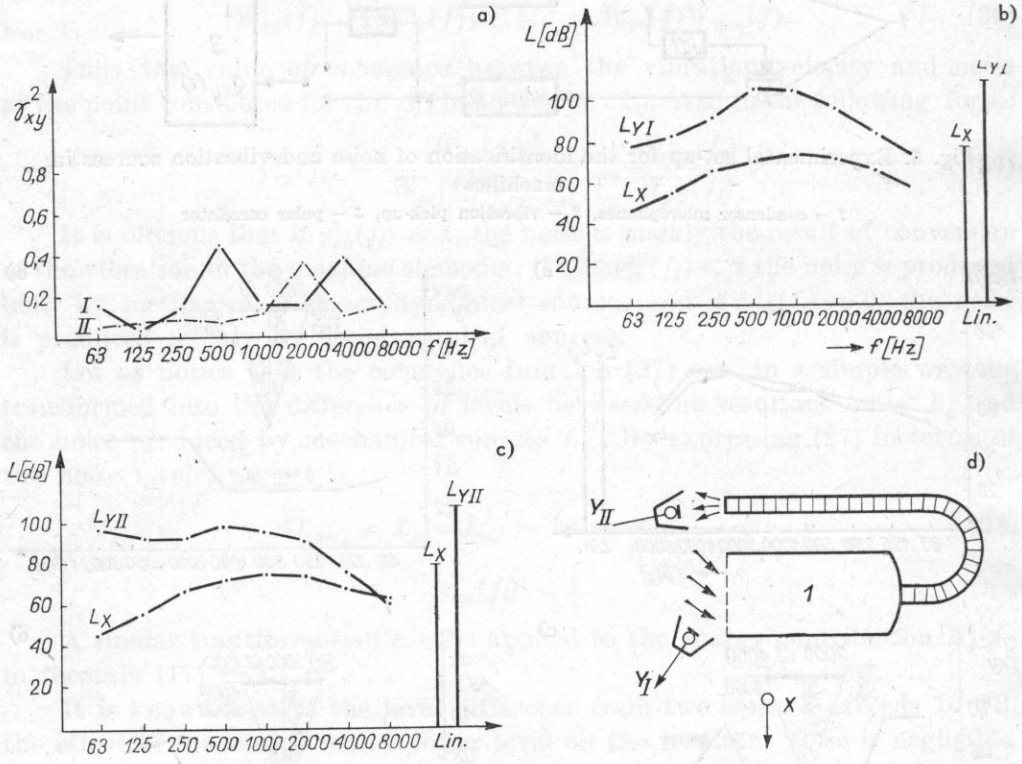

Fig. 7. *a*) Coherence of partial sources in the blower «PYE-LING», *I* – inlet, *II* – outlet, *b*) octave spectrum of noise measured at the points *X* and Y_I, *c*) octave spectrum of noise measured at the points *X* and Y_{II}, *d*) situation of microphones in the measurement according to Fig. 7: *1* – blower «PYE-LING»

Results of these experiments are shown in Figs 6a to d. Fig. 6a presents the octave-band noise spectrum measured in the channels *X* and *Y* with the microphones located on a moving base as shown in Fig. 4. It can be seen that the unweighted linear noise levels differ only slightly frome ach other. The octave levels differ to some extent although they are identical in character. Fig. 6b

presents the experimental results for the determination of the locations of the noise sources in the blower by means of the quantity $r_{xy}^{\max}$. Channel X had a unit gain flat transmittance, whereas channel Y had a band-pass transmittance for each octave filter. The opposite situation is shown in Fig. 6d, and results in which both X and Y channels had octave filters are shown in Fig. 6c. It followed from the octave band measurements that in all cases the sources were measured within the scanning angle ($\alpha = 12°$) with respect to the noise source. It is possible to observe only octave displacements related to the kind of quantity measured. However, the simplicity of the procedure and the reliability of the results showed that measurement with octave filters in both X and Y channels was preferable (Fig. 6c). For this case, according to formulae (16) and (20), $\varrho_{xy}^{\max} \approx 1$ should

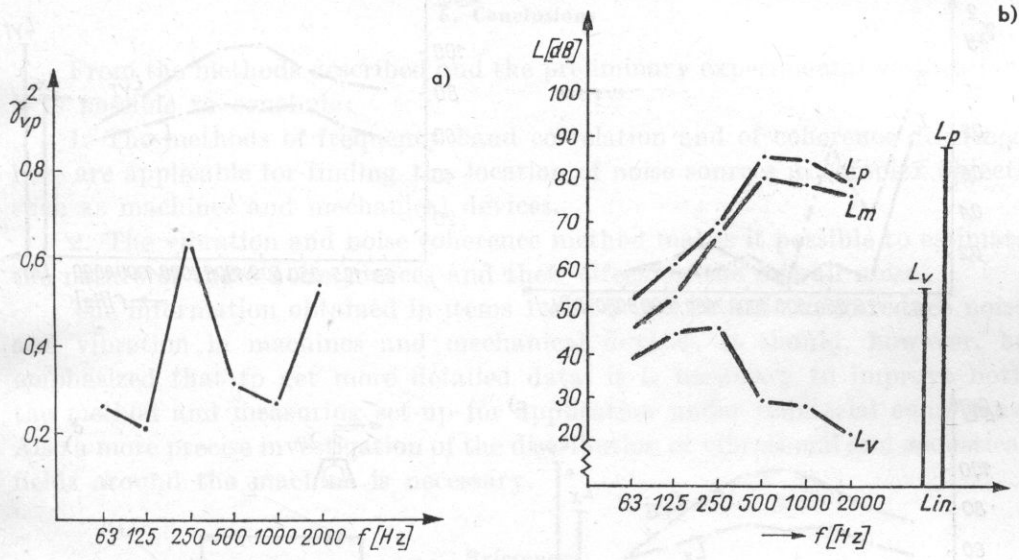

Fig. 8. a) Coherence of vibration-noise at the blower «PYE-LING», b) octave spectrum of the total noise L_p, the mechanical noise L_m and the vibration velocity L_v

be obtained. However, disturbances in the acoustic field due to the room properties make this quantity in some octave bands much less than unity. In an open space or an anechoic chamber the condition $\varrho_{xy}^{\max} \approx 1$ will be more fully realized.

Secondly, we attempted to determine the location of the same sources by means of the coherence function which was measured for two arbitary partial sources: the air inlet I and the air outlet from hose II. Figs 7a-d show the results of these experiments and the corresponding arrangement of microphones.

It follows from the diagram of the coherence function, Fig. 7a, that the blower outlet can be treated as a noise source only within the 2 kHz octave

while the blower inlet produces significant components of the resultant noise level within the 500 Hz and 4 kHz octaves.

The attempts to determine the character of the blower noise on the basis of the measured coherence between the casing vibration velocity $[v(t)]$ and the resultant noise $[p(t)]$ are illustrated in Figs 8a and 8b.

It can be seen in Fig. 8a that the radiation of mechanical noise by the vibrating casing can be recognized as significant in the 250 Hz and 2 kHz octave bands ($\gamma^2_{vp} > 0.5$) in spite of the fact that the level of vibration velocity for 2 kHz octave is low (Fig. 8b). This indicates that the vibration to noise conversion is highly efficient in this band. Fig. 8b demonstrates the spectrum of the mecha-

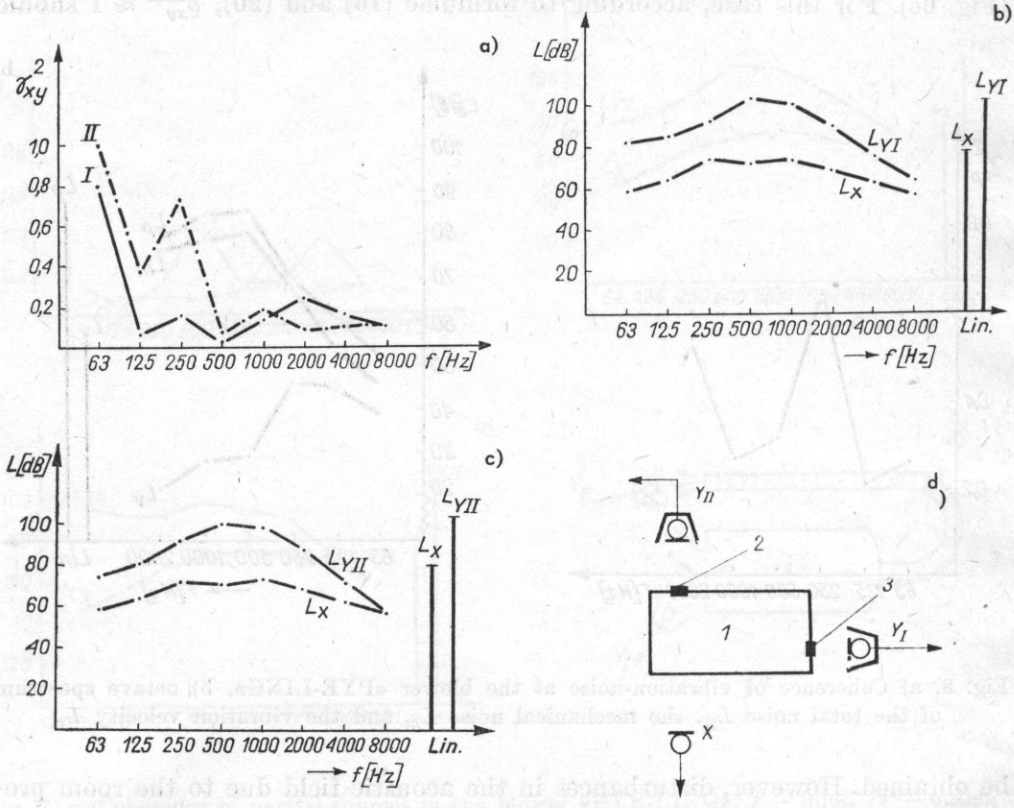

Fig. 9. a) Coherence of partial sources in the compressor, b) octave spectrum of the noise measured at the points X and Y_I, c) octave spectrum of the noise measured at the points X and Y_{II}, d) situation of microphones in the measurements according to Fig. 9
1 – single stroke compressor, *2* – air filter, *3* – electric motor

nical noise obtained by subtracting ΔL_{pm_i} (28) from the spectrum for L_{p_i}. It can be seen that the difference of levels L_{p_i} and L_{m_i} fluctuates within 5 to 7 dB outside the bands of high coherence. This fact indicates that these components are of distinct aerodynamic origin.

Attempts were also made to use the coherence method to determine locations of noise sources in the compressor, treating the filter inlet (*II*) and the electric motor ventilator (*I*) as the arbitrary noise sources. The results of these experiments and the experimental arrangement are shown in Fig. 9a to 9d. It can be seen from Fig. 9a that the inlet filter (*II*) is the main sound source for the low and medium frequencies, 63 to 250 Hz, while the motor ventilator (*I*) produces only the high frequency components, 2 to 4 kHz. The high value of coherence for 63 Hz should presumably be ascribed to the unfavourable location of the microphone Y_I which received not only the noise from the source of interest but also the low frequency components of the resultant noise in the room where the experiments were performed.

6. Conclusions

From the methods described and the preliminary experimental verification, it is possible to conclude:

1. The methods of frequency band correlation and of coherence described here are applicable for finding the location of noise sources in complex objects such as machines and mechanical devices.

2. The vibration and noise coherence method makes it possible to estimate the nature of these noise sources and their effect on the overall noise.

The information obtained in items 1 and 2 can be utilized to reduce noise and vibration in machines and mechanical devices. It should, however, be emphasized that to get more detailed data, it is necessary to improve both the method and measuring set-up for application under industrial conditions. Also a more precise investigation of the distribution of vibrational and acoustical fields around the machine is necessary.

References

[1] J. S. Bendat, A. G. Piersol, *Measurement and Analysis of Random Data*, John Wiley & Sons Inc., New York, London, Sydney 1966, ch. 5.

[2] J. Benes, *Statistical Dynamics of Automatic Control Systems*, ILIFFE Books Ltd., London 1967, p. 161-165.

[3] J. T. Broch, *On the application and limitations of the cross-correlation and the cross-spectral density techniques*, Brüel & Kjaer Technical Review, **4**, 3-27 (1970).

[4] A. K. Novikov, *Correlation measurements in ship acoustics*, (in Russian), Energia, Leningrad 1971.

[5] J. T. Broch, *Mechanical Vibration and Shock Measurements*, Brüel & Kjaer, 246-255 (1973).

[6] J. T. Broch, *On the measurement and interpretation of cross-power spectra*, Brüel & Kjaer Technical Review, 3, 3-20 (1968).

[7] K. J. Goff, *The application of correlation techniques in some acoustic measurements*, JASA, **27**, 2, 223-236 (1955).

Received 2nd March 1975

ARHIVCES OF ACOUSTICS
1, 1, 21-27 (1976)

THE EQUATION OF ACOUSTIC RAYS IN AN INHOMOGENEOUS MOVING MEDIUM

RUFIN MAKAREWICZ

Chair of Acoustics, A. Mickiewicz University (Poznań)

This paper is devoted to the derivation of the differential equations for rays in an inhomogeneous medium which moves with a velocity $\overline{W}(z)$. The velocity of sound propagation in this medium is assumed to be a function of one variable $a(z)$.

The discussion is based on the Snell's generalized law which has been derived by a new method.

1. Introduction

Let us assume that in a moving and inhomogeneous medium, an arbitrare wave surface is given by the equation $\varphi(\bar{r}, t) = 0$. This surface moves and changy its form. Then, for the time instants $t_3, t_2, t_1, \ldots$ we can write the respectve equations

$$\varphi(\bar{r}, t_1) = 0, \ \varphi(\bar{r}, t_2) = 0, \ \varphi(\bar{r}, t_3) = 0, \ldots$$

Then we have the relation of the form $t = \psi(\bar{r})$. If the sound velocity at a point determined by the vector $\bar{r}$ is $a(\bar{r})$ and the medium moves with a velocity $\overline{W}(\bar{r})$, then $\psi(\bar{r})$ satisfies the so-called generalized eikonal equation [3] which can be written in the form

$$H\left(x, y, z, \frac{\partial\psi}{\partial x}, \frac{\partial\psi}{\partial y}, \frac{\partial\psi}{\partial z}\right) = 0.$$

Solution of this equation takes the form of a set of partial differential equations describing a family of curves which are orthogonal to the surface $t = \psi(\bar{r})$ [14]. These curves represent rays. The same set of equations is obtainable either by starting from the fundamental equations of hydrodynamics [12, 13] or by constructing the Hamilton equations [5, 7], as is the case in optics.

The simple way for deriving the equations of rays is based on the generalized Snell's law. This paper presents a new method for deriving this law in the case of a layered medium.

The differential equations thus obtained can be integrated if the functions $a(z)$ and $W_x(z)$, $W_y(z)$, $W_z(z)$ are given. Such an integration has been accom-

plished for the case of medium at rest $\overline{W}(z) \equiv 0$, with the sound velocity being linearly dependent on the coordinate $a(z) = a_0(1 - \beta z)$.

2. The Snellius generalized equation

Wilibrord SNELL (SNELLIUS, 1591-1626) established experimentally the direction of the way in which propagated wave varies with a discrete change in sound velocity.

The generalized SNELL'S law determines how the direction of propagation changes in a moving medium with the sound velocity being varied continuously.

There are several ways of deriving the generalized SNELL'S law [1, 2, 4, 6, 8, 9, 10]. The method presented in this paper seems to be simpler than the others.

WARREN [15] presents a number of works in which the SNELL'S law was derived wrongly.

In an immobile medium, the form of the wave surface is a function of the propagation velocity $\bar{a} = \bar{n}a(\bar{r})$ ($\bar{n}$ — unit vector perpendicular to the wave surface) and initial conditions. If we assume that the medium moves with velocity $\overline{W}(\bar{r})$, then the resultant propagation velocity of disturbance is

$$\overline{U} = \bar{n}a(\bar{r}) + \overline{W}(\bar{r}). \tag{1}$$

The form of the wave surface depends only on the velocity component $\overline{U}$ perpendicular to this surface

$$\overline{U}_n = \bar{n}[a(\bar{r}) + \bar{n}\,\overline{W}(\bar{r})].$$

The component $\overline{U}_{||}$ parallel to the wave surface causes an arbitrary acoustic particle to move over this surface and contributes nothing to the physical pattern of the phenomenon (Fig. 1).

Let us assume that the medium is layered, that is, each of its parameters and thus the propagation velocity $a(z)$ and the velocity of the medium $\overline{W}(z)$ are

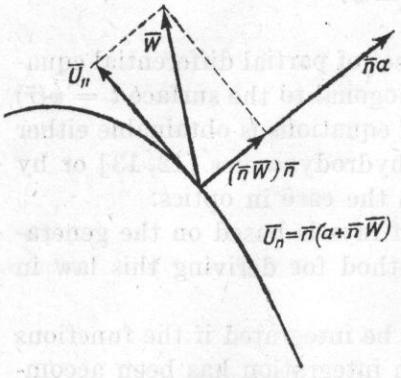

Fig. 1. Components $\overline{U}_{||}$ and $\overline{U}_n$ efvelocity $\overline{U} = \bar{n}a + \overline{W}$

functions of only one variable. In order to derive the generalized SNELL'S law let us assume additionally that this medium is formed of layers Δz thick, within which the velocity of the moving medium, the velocity of sound and the unit vector $\bar{n}$ are constant, but differ (Fig. 2) from layer to layer.

The ray corresponding to the wave propagating in such a medium is a broken line and the phase in the k-th layer is

$$\psi = t + \left(\frac{\bar{n}\bar{r}}{a + \bar{W}\bar{n}}\right)_k,$$

where (Fig. 2) $\bar{n}_k$ – unit vector perpendicular to the wave surface, a_k – sound

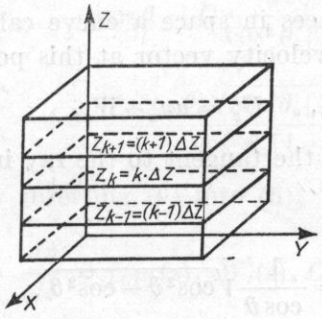

$$\left\{\bar{W}_{k+1}=\bar{W}\left[(k+1)\cdot\Delta z\right], a_{k+1}=a\left[(k+1)\Delta z\right], \bar{n}_{k+1}=\bar{n}\left[(k+1)\Delta z\right]\right\}$$
$$\left\{\bar{W}_k=\bar{W}\left[k\cdot\Delta z\right], a_k=a\left[k\cdot\Delta z\right], \bar{n}_k=\bar{n}\left[k\cdot\Delta z\right]\right\}$$

Fig. 2. Model of a medium consisting of layers

velocity, $\bar{W}_k$ – velocity of the moving medium in the k-th layer, and $\bar{r}_k$ – vector of the form

$$\bar{r}_k = (x - x_{k-1})\bar{i} + (y - y_{k-1})\bar{j} + (z - z_{k-1})\bar{k}.$$

The phases in the plane of contact of two layers at a point $\bar{r} = x\bar{i} + y\bar{j} + \Delta z\bar{k}$ must be equal to each other at an arbitrary time instant

$$t + \left(\frac{\bar{n}}{a + \bar{W}\bar{n}}\right)_{k+1} \bar{r} = t + \left(\frac{\bar{n}}{a + \bar{W}\bar{n}}\right)_k \bar{r}. \tag{2}$$

This expression can be written in the following form

$$\left[\left(\frac{n_x}{a + \bar{W}\bar{n}}\right)_{k+1} - \left(\frac{n_x}{a + \bar{W}\bar{n}}\right)_k\right] x + \left[\left(\frac{n_y}{a + \bar{W}\bar{n}}\right)_{k+1} - \left(\frac{n_y}{a + \bar{W}\bar{n}}\right)_k\right] y +$$
$$+ \left[\left(\frac{n_z}{a + \bar{W}\bar{n}}\right)_{k+1} - \left(\frac{n_z}{a + \bar{W}\bar{n}}\right)_k\right] \Delta z = 0.$$

Assuming $\Delta z \to 0$, we obtain

$$\frac{d}{dz}\left(\frac{n_x}{a + \bar{W}\bar{n}}\right) = 0, \quad \frac{d}{dz}\left(\frac{n_y}{a + \bar{W}\bar{n}}\right) = 0.$$

The expressions

$$\frac{n_x}{a(z)+W_x(z)n_x+W_y(z)n_y+W_z(z)n_z}=C_1$$
$$\frac{n_y}{a(z)+W_x(z)n_x+W_y(z)n_y+W_z(z)n_z}=C_2 \tag{3}$$

describe the generalized SNELL'S law for a layered medium.

3. The differential equations of rays

An arbitrary point of the wave front traces in space a curve called the ray. According to (1) the components of the velocity vector at this point are

$$U_x=an_x+W_x,\qquad U_y=an_y+W_y,\qquad U_z=an_z+W_z, \tag{4}$$

where n_x, n_y, n_z are the directional cosines of the tangent to the ray in a immobile medium.

From Fig. 3 it follows that

$$n_x=\cos\theta,\qquad n_y=\cos\theta\tan\vartheta,\qquad n_z=\frac{1}{\cos\vartheta}\sqrt{\cos^2\vartheta-\cos^2\theta}\,.$$

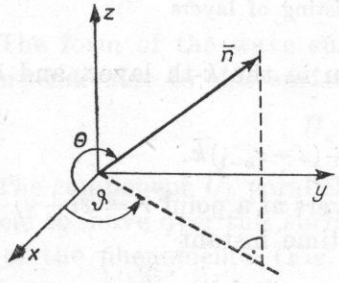

Fig. 3. Determination of vector $\bar{n}$ by means of angles θ, ϑ

By substituting the directional cosines expressed in such a way into (4) and taking into account that

$$U_x=\frac{dx}{dt},\qquad U_y=\frac{dy}{dt},\qquad U_z=\frac{dz}{dt}$$

we obtain the differential equations of the ray

$$\frac{dx}{dz}=\frac{[a(z)\cos\theta+W_x(z)]\cos\vartheta}{a(z)\sqrt{\cos^2\vartheta-\cos^2\theta}+W_z(z)\cos\vartheta},$$
$$\frac{dy}{dz}=\frac{[a(z)\cos\theta\tan\vartheta+W_y(z)]\cos\vartheta}{a(z)\sqrt{\cos^2\vartheta-\cos^2\theta}+W_z(z)\cos\vartheta}. \tag{5}$$

To perform the integration effectively, it is necessary to know the relations $\theta = \theta(z)$ and $\vartheta = \vartheta(z)$ in which x, y are not involved because the medium is layered along the direction of axis z. From (3), we get

$$\operatorname{tg}\vartheta = C_2/C_1,$$

$$\cos\theta = C_1 \frac{a[1-(W_xC_1+W_yC_2)] \pm W_z\sqrt{[1-(W_xC_1+W_yC_2)]^2-(a^2-W_z^2)(C_1^2+C_2^2)}}{[1-(W_xC_1+W_yC_2)]^2+W_z^2(C_1^2+C_2^2)}.$$

Instead of C_2, it is convenient to assume $\vartheta = \vartheta_0$ as a constant and to denote $C = C_1$

$$\cos\theta = C \frac{a\cos^2\vartheta_0[1-C(W_x+W_y\tan\vartheta_0)]}{\cos^2\vartheta_0[1-C(W_x+W_y\tan\vartheta_0)]^2+W_z^2C^2} +$$

$$+C \frac{W_z\cos\vartheta_0\sqrt{\cos^2\vartheta_0[1-C(W_x+W_y\tan\vartheta_0)]^2-(a^2-W_z^2)C^2}}{\cos^2\vartheta_0[1-C(W_x+W_y\tan\vartheta_0)]^2+W_z^2C^2}.$$

By inserting (6) into (5), we obtain

$$\frac{dx}{dz} = f_1\{a(z),\ W_i(z),\ C,\ \vartheta_0\}, \qquad \frac{dy}{dz} = f_2\{)vz),\ W_i(z),\ C,\ \vartheta_0\}. \tag{7}$$

These equations are integrable. The constants C and ϑ_0 depend on the direction of the ray θ, ϑ_0 in the neighbourhood of the source (Fig. 3).

If the source is located at the point (x_0, y_0, z_0), then we obtain C from (3) as a function of the angles θ_0 and ϑ_0 and quantities a, $\overline{W}$ taken for $z = z_0$

$$C = \frac{\cos\theta_0\cos\vartheta_0}{\cos\vartheta_0[a(z_0)+W_x(z_0)\cos\theta_0]+W_y(z_0)\cos\theta_0\sin\vartheta_0+W_z(z_0)\sqrt{\cos^2\vartheta_0-\cos^2\theta_0}}. \tag{8}$$

4. The explicit form of the equations of rays

Integration of (7) with given functions $\overline{W}(z)$, $a(z)$ and under the assumptions that the coordinates of the source are x_0, y_0, z_0 provides the following equations for the rays:

$$x = x_0 + \int_{z_0}^{z} f_1\{a(z),\ W_i(z),\ a(z_0),\ W_i(z_0),\ \vartheta_0,\ \theta_0\}\,dz,$$
$$y = y_0 + \int_{z_0}^{z} f_2\{a(z),\ W_i(z),\ a(z_0),\ W_i(z_0),\ \vartheta_0,\ \theta_0\}\,dz. \tag{9}$$

Example. Formulae (9) are usually so complex that the integration can be accomplished only in a numerical way. In some cases, it is possible to

perform this integration directly and to obtain the equations of rays of the form $x = F_1(z)$, $y = F_2(z)$.

If we assume, for instance, that the medium is at rest, that is $\overline{W}(z) = 0$ and the sound velocity is a function of the form $a(z) = a_0(1-\beta z)$, then from (6) we have

$$\cos\theta = Ca_0(1-\beta z),$$

and the set of equation (7) simplifies to the form

$$\begin{aligned} \frac{dx}{dz} &= \frac{Ca_0(1-\beta z)\cos\vartheta_0}{\sqrt{\cos^2\vartheta_0 - C^2a_0^2(-\beta z)^2}}, \\ \frac{dy}{dz} &= \frac{Ca_0(1-\beta z)\sin\vartheta_0}{\sqrt{\cos^2\vartheta_0 - C^2a_0^2(1-\beta z)^2}}. \end{aligned} \tag{7'}$$

From (8), we obtain

$$C = \frac{\cos\theta_0}{a_0(1-\beta z_0)}$$

and after integration of (7) we can write

$$\begin{aligned} x &= x_0 + \frac{\cos\vartheta_0(1-\beta z_0)}{\cos\theta_0\beta}\left[\sqrt{\cos^2\vartheta_0 - \cos^2\theta_0} - \sqrt{\cos^2\vartheta_0 - \frac{\cos^2\theta_0}{(1-\beta z_0)^2}(1-\beta z)^2}\right], \\ y &= y_0 + \frac{\sin\vartheta_0(1-\beta z_0)}{\cos\theta_0\beta}\left[\sqrt{\cos^2\vartheta_0 - \cos^2\theta_0} - \sqrt{\cos^2\vartheta_0 - \frac{\cos^2\theta_0}{(1-\beta z_0)^2}(1-\beta z)^2}\right]. \end{aligned} \tag{9'}$$

It can be shown that the set of equations (9') describes a circle that lies in a plane perpendicular to the plane (x, y) and passes through the point (x_0, y_0, z_0) [11].

5. Conclusions

The typical layered medium is the atmosphere. It can be assumed that the velocity of motion of this medium ($\overline{W}(z)$ — velocity of the wind) and the sound velocity $a(z)$ are functions of the altitude.

Under such assumptions, the formulae (9) are equations of acoustic rays in the atmosphere when the wind blows, while (9') is the set of he same equations when the atmosphere is at rest.

Equations (9) can be utilized to investigate e.g. the phenomenon of refraction under a variety of atmospheric conditions or to the determine the location of sonic booms on the ground.

Acknowledgement. I am very indebted to Prof. H. RYFFERT for very helpful discussion and remarks.

References

[1] A. Biestek, *The analysis and methods for determining the propagation of sound explosions* (in Polish), Postępy Astronautyki, **3**, 89-124 (1969).

[2] A. Biestek, *Acoustic explosions in inhomogeneous atmosphere* (in Polish), Postępy Astronautyki, **2**, 59-72 (1970).

[3] D. I. Blokhincev, *Acoustics of a nonhomogeneous moving medium*, JASA, 18, 322-328 (1946).

[4] E. H. Barton, *On the refraction of sound by wind*, Phil. Mag., **1** (1901).

[5] C. I. Chessel, *On three-dimensional acoustic-ray tracing in an inhomogeneous anisotroping atmosphere using Hamiltons equation*, JASA, **53**, 83-87 (1973).

[6] S. Fujiwhara, *On the abnormal propagation of sound waves in the atmosphere*, Bull. Centr. Met. Obs. Tokyo, **2** (1916).

[7] J. Haselgrove, *Ray theory and a new method for ray tracing*, Rep. of Conf. on Physics of Ionosphere, London Physical Society, London 1954.

[8] E. T. Kornhauser, *Ray theory for moving fluid*, JASA, 945-949 (1953).

[9] J. Lighthill, *The propagation of sound through moving fluids*, J. Sound a Vibr., **24**, 471-493 (1972).

[10] E. A. Milne, *Sound waves in the atmosphere*, Phil. Mag., **17**, 96-114 (1921).

[11] R. Makarewicz, *The equation of acoustic ray in inhomogeneous moving medium* (in Polish), Proceedings of 20th Open Seminar on Acoustics. Part I, 194-196, Poznań 1973.

[12] L. K. Szubert, *Numerical study of sound refraction by jet flow*, JASA, **51**, 439-446 (1972).

[13] R. J. Thompson, *Ray theory for an inhomogeneous moving medium*, JASA, **51**, 1675-1682 (1972).

[14] P. Ugincius, *Ray acoustic and Fermat's principle in a moving inhomogeneous medium*, JASA, **51**, 1759-1763 (1972).

[15] C. H. E. Warren, *A note on the refraction of sound in a moving gas*, J. Sound Vibr., **1**, 175-178 (1964).

Received 27th January 1975

ARCHIVES OF ACOUSTIC
1, 1, 29-32 (1976)

ON THE POSSIBILITY OF AN INVESTIGATION OF SEMI-CONDUCTOR SURFACE PROPERTIES USING ULTRASONIC SURFACE WAVES

ALEKSANDER OPILSKI

Institute of Physics, Silesian Technical University (Gliwice)

The investigations concerning the propagation of surface waves have so far neglected semiconductors. The present paper points out the necessity of taking into account the effect of surface properties on the propagation of surface waves, even for long ultrasonic waves such that $\lambda \gg r_D$ (λ – wavelength and r_D – Debye radius). Having this in mind some possibilities of determining the electrostatic potential on the basis of acoustical data obtained for the solid material and thin semiconductor layers have been described.

It is possible to calculate the electrostatic potential developed at a thin surface layer which is perturbed by the surface wave, in terms of acoustical data obtained for the bulk material. It is well known that the energy levels of the surface potential are curved and this fact influences the other surface properties of the semiconductors. This curvature is determined from the field effect i.e. when the curve representing the dependence of surface conductivity on applied voltage reaches a minimum.

If the external applied field is shielded by the field associated with the surface states, then the minimum of surface conductivity may not be obtainable and the application of the field effect method is restricted. Other methods require certain models to be assumed for the surface states and they thus provide only indirect information.

Surface wave research suggests new possibilities for the determination of surface potential and surface states. In a piezoelectric medium the surface wave will give rise to a travelling electric field and this in turn is capable of interacting with electrons in the medium of a piezosemiconductor or of medium in contact with a pure piezoelectric.

The following special cases will be considered:

1. The wave is excited in a piezoelectric medium which also exhibits semiconductor properties. The surface wave in this case penetrates into the medium to a depth of the order of a wavelength. Since the thickness of the

layer close to the surface is of the order of the Debye's radius r_D, the surface layer is capable of effecting the surface wave only if $\lambda \leqslant r_D$ (discussed in [2]).

2. The wave propagates in a piezoelectric medium and its accompanying electric field penetrates into the semiconductor which has no acoustical contact with the piezoelectric. The field penetrates into the semiconductor to a depth equal to r_D from the surface. Then the wave propagation parameters depend only on the properties of this layer.

3. The surface wave propagates in the piezoelectric onto which a semiconductor layer of thickness $d \approx r_D$ is deposited, where $r_D \ll \lambda$. If the semiconductor shows no piezoelectric effect, the wave interacts with the carriers through the field generated in the piezoelectric substrate. We do not consider here the interaction through the deformation potential since at low frequencies it is extremely small. In the case of a piezosemiconductor layer, the layer surface is capable of affecting propagation only if the layer thickness $d \approx r_D$, where $\lambda \gg r_D$.

We can use cases 2 and 3 to investigate the properties of the layer close to the surface of solid semiconductors or thin semiconductor layers.

Let us consider a potential barrier corresponding to small absolute values of the electrostatic surface potential $Y_s \ll 1$. In this case, the change in the space charge in the interface layer is also small. The changes in potential are small compared to kT/e, while the properties of the region of the space charge differ only a little from those of the unperturbed portion of the semiconductor. Our discussion was intended to demonstrate the possibility of employing the surface wave for investigating the interface layer. The problem was restricted to considering the effect of the space charge distribution in the interface layer, i.e. the layer close to surface, on the attenuation coefficient α of the surface wave.

The attenuation coefficient for case 2 can be described by the expression

$$\alpha = \eta k F \frac{\varepsilon_1}{\varepsilon_2} \frac{\omega' \tau_M \gamma}{1 + \omega'^2 \tau_M^2 \left(1 + \frac{\varepsilon_1}{\varepsilon_2}\right)^2 \gamma^2}, \tag{1}$$

where η — electromechanical coupling constant, $k = 2\pi/\lambda$ — wave number, F — positive number which depends slightly on piezoelectric modulus, ε_1, ε_2, ε_0 — permittivities of the substrate, the semiconductor and the vacuum respectively, $\tau = \varepsilon_2 \varepsilon_0 / \sigma = \tau_M$ — Maxwell relaxation time for a semiconductor, $\omega = 2\pi\nu - \nu$ denotes frequency, σ — specific conductivity, $\gamma = 1 - f\mu E_0 / v_s$, $\omega' = \omega - k v_d$, where v_d — drift velocity and v_s — propagation velocity, μ — mobility and E_0 — the drift field.

It should be taken into account that, in the case under consideration, the carrier concentration is a function of the penetration depth n_0 in the semiconductor without the electrical field which accompanies the acoustic wave. For

this reason, we should determine the average value of the electric conductivity $\langle\sigma\rangle$, which determines the absorption of acoustical energy.

In the layer close to the surface for $Y_s \ll 1$, the electrostatic potential is given by the following function of the depth

$$Y = Y_s \exp(-z/r_D), \tag{2}$$

where

$$r_D = \left[\frac{\varepsilon\varepsilon_0 k\sigma}{2\pi e^2(n_0+p_0)}\right]^{1/2}.$$

The carrier concentration is expressed as follows:

$$n_0(z) = n_\infty(1 - Y_s e^{-z/r_D}). \tag{3}$$

Then

$$\langle\sigma\rangle = \left[\frac{1}{r_D}\int_0^{r_D} n_{00}(1 - Y_s e^{-z/r_D})\,dz\right] e\mu. \tag{4}$$

The corresponding calculated field

$$\langle\vec{\sigma}\rangle = \sigma(1 - 0.6\,Y_s). \tag{5}$$

Insertion of (5) into (1) provides

$$\alpha = \eta k F \frac{\varepsilon_1}{\varepsilon_2} \frac{\omega'\tau_M(1 - 0.6\,Y_s)\gamma}{1 + \omega^2\tau_M^2(1 + 1.2\,Y_s)\left(1 + \dfrac{\varepsilon_1}{\varepsilon_2}\right)^2\gamma^2}. \tag{6}$$

It follows from (6) that the attenuation coefficient α is related to the electrostatic surface potential. Hence, from measurements of the attenuation coefficient resulting from the interaction between the surface wave and electrons it is possible to determine how the energy bands are curved on the semiconductor surface.

We can suggest here the following procedures:

1. The surface potential is determined directly from measurements of the attenuation coefficient. To do this, we have to know the remaining quantities involved in (6) which describe the semiconductor properties.

2. In order to determine the surface potential, we change the frequency or the conductivity in the bulk of the semiconductor and make use of the relation between these quantities and the attenuation coefficient.

The curves $\alpha = \alpha(\omega)$ and $\alpha = \alpha(\sigma)$ have maximum values at positions depending on the magnitude of the curvature of the energy bands.

Thus the curve $\alpha = \alpha(\omega)$ has its maximum at

$$\omega = \frac{1 - 0.6\,Y_s}{\tau_M\left(1 + \dfrac{\varepsilon_1}{\varepsilon_2}\right)}, \tag{7}$$

while for the curve $\alpha = \alpha(\sigma)$ it is at

$$\sigma = \omega(\varepsilon_1 + \varepsilon_2)(1 + 0.6 Y_s). \tag{8}$$

3. The maximum of the curve $\alpha = \alpha(\gamma)$ (8) occurs when

$$\gamma = (1 + 0.6 Y_s)/\omega\tau_M.$$

Conclusions

It follows from the above discussion that the method of ultrasonic surface waves (including also the case $\lambda \gg r_D$) can be employed for determining the electrostatic surface potential in solid semiconductors and thin semiconductor layers. Various measuring methods are used. Their choice depends on what quantities are known characterizing the bulk properties of the semiconductor.

References

[1] D. R. Frankl, *Electrical properties of a semiconductor surface*, Pergamon Press, 1967.
[2] S. Zenon, E. M. Conwell, Appl. Phys. Lett., **5**, 17, 218-220 (1970).
[3] Y. V. Gulayev, Physics of Solids, **9**, 12, 2595 (1970).
[4] J. A. Viktorov, A. A. Talaschev, Akust. Zh., **18**, 2, 197 (1972).
[5] A. A. Karpuschin, S. K. Savinykh, Physics of Solid, **4**, 9, 114 (1967).
[6] A. Many, Y. Goldstein, N. B. Grover, *Semiconductor surfaces*, North-Holland Publ. Comp., 1971.

Received 6th January 1975

ARCHIVES OF ACOUSTICS
1, 1, 33-41 (1976)

ON AN APPROXIMATE METHOD FOR CALCULATING FILTERS BASED ON ACOUSTIC SURFACE WAVES

ZENON CEROWSKI, ALEKSANDER OPILSKI,
TADEUSZ PUSTELNY, MARIAN URBAŃCZYK

Institute of Physics, Silesian Technical University (Gliwice)

The work describes an electric filter consisting of interdigital transducers deposited on piezoelectric substrate. A method has been presented for computing the transducer parameters with an assumed amplitude-frequency characteristic.

The filters produced on the basis of calculated transducer parameters were tested and the results are given in this paper.

1. Discussion on transducers

The possibility of constructing devices based on the phenomenon of the propagation of elastic waves in a solid created considerable interest in the analysis of interdigital transducers.

There are a few methods employed for analyzing transducers, for example the method of an equivalent circuit [1, 5, 6] and that of strips.

One of the most convenient methods, because of its simplicity and reliability, is to calculate the form of an amplitude-frequency characteristic for a given shape of transducer as proposed by TANCRELL and HOLLAND [1]. This procedure is relatively simple but it requires repeated calculations by trial and error.

In this procedure it is assumed that a period of an alternating acoustical field is equal to a period of electrical field gradient. Since the electric field gradient is non-uniform an approximate assumption is that the energy sources appear only on the edge of each electrode and, therefore, they can be described by the function δ (Fig. 1).

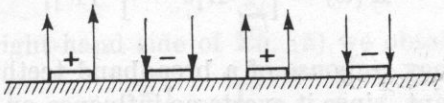

Fig. 1. The electric field gradient at the edges of electrodes

The frequency response of the transducer in this case is described by the expression

$$\sum_{l=-\infty}^{l=+\infty} \frac{r(x_l)}{4z'(x_l)} \cos\left[\frac{\pi}{2}e - \frac{\pi}{4}\right] e^{-ikx_l}$$

$$= \int_{-\infty}^{+\infty} \left\{ r(x_l) \cos\left[2\pi z(x) - \frac{\pi}{4}\right] e^{-ikx} \right\} dx + \quad \text{1st harmonic}$$

$$+ \int_{-\infty}^{+\infty} \left\{ r(x_l) \cos\left[6\pi z(x) - \frac{\pi}{4}\right] e^{-ikx} \right\} dx + \quad \text{3rd harmonic}$$

$$+ \int_{-\infty}^{+\infty} \left\{ r(x_l) \cos\left[10 z(x) - \frac{\pi}{4}\right] e^{-ikx} \right\} dx + \ldots \quad \text{5th harmonic} \qquad (1)$$

where $k = \omega/v$, ω is the angular frequency, v — propagation velocity of the surface wave, l — number of successive edges on the transducer, $r(x)$ — function of electrode overlapping, the envelope of mutual penetration, $z(x)$ — function of the number of electrode pairs, $2z'(x) = 2dz(x)/dx$ the density of electrodes.

It follows from the above analysis that the higher odd harmonics will be present with the fundamental.

The frequency transmittance of a system consisting of one transmitting and one receiving transducer takes the form

$$H(\omega) = \frac{U(\omega)}{U(\omega)} = \sum_{k=1}^{K} \sum_{l=1}^{L} A_k A_l e^{i(x_l - X_k)\frac{\omega}{v}}, \qquad (2)$$

where K is the total number of edges in the receiver, L — total number of edges in the transmitter, x_l — distance between the lth edge in the transmitter and the beginning of the transducer, X_k — distance between the kth edge in the receiver and the beginning of the transmitting transducer, A_k, A_l — coefficients depending on the geometry of electrodes; these are functions of the phase and the electrical field gradient.

For a system of two transducers in which one is a broadband unit with a small number of electrodes, while the other is a narrowband unit with a complex structure of electrodes, the function $H(\omega)$ can be expressed as follows

$$H(\omega) = \left[\sum_{l=1}^{l} A_l e^{-ikx_l}\right] \; [F], \qquad (3)$$

where $[F]$ is a frequency response of a broadband teeth arrangement that can be treated as a constant, since it exerts no influence on the frequency characteristics of the system. The transmission band of the transmitting transducer

is comprised within the transmission band of the receiving transducer. As follows from expression (3) there exists in this case a direct relation between Fourier transformation of the teeth arrangement mode and the transmittance $H(\omega)$.

2. Computation of the data for filter designing

The purpose of the present work is to propose a modification of the method [1] employed for computing filters based on acoustical surface waves.

This modification consists of computing the transducer shape corresponding to the a priori assumed amplitude-frequency characteristics.

Let us determine such a function to overlap the digits of an interdigital transducer operating in conjunction with a broadband transducer such that the frequency transmittance is of the form

$$H(\omega) = \begin{cases} C & \text{for } \omega_1 < \omega < \omega_2, \\ 0 & \text{for remaining range,} \end{cases}$$

where ω_0 is the resonance frequency, and ω_2, ω_1 — upper and lower frequency limits, respectively.

This discussion concerns only the fundamental frequency. According to (1) we have

$$\begin{aligned} H(\omega) &= \sum_{l=-\infty}^{l=\infty} \frac{r(x_l)}{4z'(x_l)} \cos\left[\frac{\pi}{2} l - \frac{\pi}{4}\right] e^{-ikx_l} \\ &= \int_{-\infty}^{+\infty} r(x) \cos\left[2\pi z(x) - \frac{\pi}{4}\right] e^{-ikx}\, dx \\ &= \int_{-\infty}^{+\infty} r(x) \cos\left[2\pi z(x) - \frac{\pi}{4}\right] e^{-ikx} v\, dt. \end{aligned} \tag{4}$$

The inverse Fourier transformation of the above expression gives

$$\begin{aligned} r(x) v \cos\left[2\pi z(x) - \frac{\pi}{4}\right] &= \frac{1}{2\pi} \int_{-\infty}^{+\infty} H(x) e^{i\omega t}\, d\omega = \frac{1}{2\pi} \int_{\omega_1}^{\omega_2} C e^{i\omega t}\, d\omega, \\ r(x) v \cos\left[2\pi z(x) - \frac{\pi}{4}\right] &= \frac{iC}{2\pi t} [e^{i\omega_2 t} - e^{i\omega_1 t}]. \end{aligned} \tag{5}$$

By developing the right-hand side of Eq. (5) we obtain

$$r(x) v \cos\left[2\pi z(x) - \frac{\pi}{4}\right] = \frac{C}{\pi v t} [\sin \omega_2 t - \sin \omega_1 t], \tag{6}$$

and this gives the following set of equations

$$r(x) = \frac{C}{\pi v t} \sin \frac{\omega_2 - \omega_1}{2v} t, \tag{7a}$$

$$\cos\left[2\pi z(x) - \frac{\pi}{4}\right] = \cos \frac{\omega_1 + \omega_2}{2v} x, \tag{7b}$$

where $t = x/v$.

It follows from (7a) and (7b) that in order tc satisfy the condition (4) the envelope of electrode overlap and the function of a number of electrode pairs should take the form

$$r(x) = \frac{C\Delta\omega}{2\pi v} \frac{\sin Bx}{Bx}, \tag{8}$$

where

$$B = \frac{\Delta\omega}{2v}, \quad z(x) = \frac{\omega_0}{2\pi v} x + \frac{1}{8}, \quad z'(x) = \frac{\omega_0}{2\pi v} = \frac{1}{\lambda} = \text{const}. \tag{9}$$

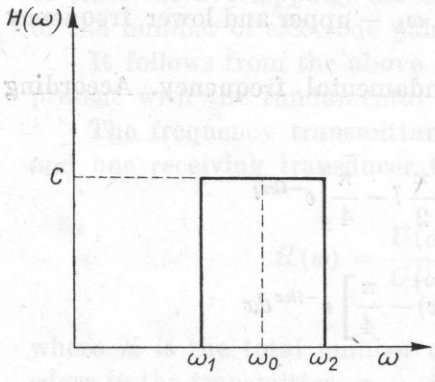

Fig. 2. The rectangular characteristics of a filter

Expression (9) shows that the transducer is non-dispersive

$$z(x) = \frac{l}{m} = \frac{l}{4} = \frac{\omega_0}{2\pi v} x_l + \frac{1}{8}, \tag{10}$$

where m is the number of edges per period, and hence

$$x_l = \frac{2\pi v}{\omega_0}\left(\frac{l}{4} + \frac{1}{8}\right) \tag{11}$$

for $l = 0, 1, 2, \ldots$

If the width of electrodes is equal to the gap between them, then

$$x_l - x_{l-1} = \frac{v}{4\omega_0} 2\pi. \tag{12}$$

The electrodes are reversed at the points at which the amplitudes D_n [1] are equal to zero

$$D_n = \pm \frac{1}{\sqrt{2}} \frac{r(x_n)v}{4z'(x_n)_r}. \tag{13}$$

Taking into account Eqs. (8) and (9), we obtain the expression

$$D_n = \pm \frac{\pi}{2\sqrt{2}} \frac{v^2}{\omega_0} \frac{\sin\left(\frac{\Delta\omega}{2v} x\right)}{\frac{\Delta\omega}{2v} x}. \tag{14}$$

For $D_n = 0$ the following is valid:

$$\frac{\sin\left(\frac{\Delta\omega}{2v} x\right)}{\frac{\Delta\omega}{2v} x} = 0$$

Hence for

$$\frac{\Delta\omega}{2v} x \neq 0 \tag{15}$$

we have

$$\sin\left(\frac{\Delta\omega}{2v} x\right) = 0. \tag{16}$$

The roots of Eq. (15) are determined by

$$x_n = n \frac{2\pi v}{\Delta v}, \quad n = 1, 2, 3, \ldots \tag{17}$$

We see then that if we need a system with a rectangular transmittance $H(\omega)$ the method provides all data necessary for designing the appropriate transducers. This fact is important because in practice we are frequently interested in systems with such amplitude-frequency characteristics.

Fig. 3. Wideband transducer of the type $(\sin x)/x$

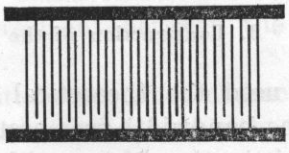

Fig. 4. Non-dispersive interdigital transducer with equally overlapping electrodes

We have also found the function for the overlapping teeth of an interdigital transducer (operating in conjunction with a broadband transducer) such that the frequency transmittance of the system is of the form

$$H(\omega) = A \frac{\sin a\omega}{a\omega}, \tag{18}$$

where A and a are constants.

From (1), taking into account only fundamental harmonics, we obtain

$$H(\omega) = \int_{-\infty}^{+\infty} r(x) \cos\left[2\pi z(x) - \frac{\pi}{4}\right] e^{-ikx} dx.$$

The inverse transformation has the form

$$r(x) v \cos\left[2\pi z(x) - \frac{\pi}{4}\right] = \frac{1}{2\pi} \int_{-\infty}^{+\infty} H(\omega) e^{i\omega t} d\omega$$

$$= \frac{1}{2\pi} \int_{-\infty}^{+\infty} A \frac{\sin a\omega}{a\omega} e^{i\omega t} d\omega. \tag{19}$$

By integration we get

$$r(x) v \cos\left[2\pi z(x) - \frac{\pi}{4}\right] = -\frac{iA}{4\pi a} 2\pi i = \frac{A}{2a}. \tag{20}$$

If an interdigital transducer is non-dispersive and its width of electrodes and the distance etween them are constant, then $\cos[2\pi z(x) - \pi/4]$ is also a constant.

In this case, the function of overlap of electrodes is also constant. We thus arrive at the conclusion that the filter consisting of non-dispersive transducers with constant overlapping digits (Fig. 4) has a frequency characteristic of the type $A(\sin a\omega/a\omega)$.

3. Construction of the filter and measurement of its characteristics

We used the theoretical studies to design and construct a broadband filter. The bandwidth was assumed to be 4 MHz. The filter was composed of a transmitting transducer with 19 pairs of electrodes and overlapping function of the type $(\sin x)/x$ (Fig. 3) and a receiving transducer with a broadband characteristic composed of 5 pairs of identical overlapping electrodes.

The maximum length of the electrodes was 6 mm, and the width of an electrode was 50 μm.

The transducers were deposited, using a photolithographic technique, onto a substrate made of piezoelectric ceramics of type PP-6. The attenuation of the input signal (in the transmission band of the system of the transducers spaced at a distance of 5 mm from each other) was 25 dB.

The results of the experiments are illustrated in Fig. 5.

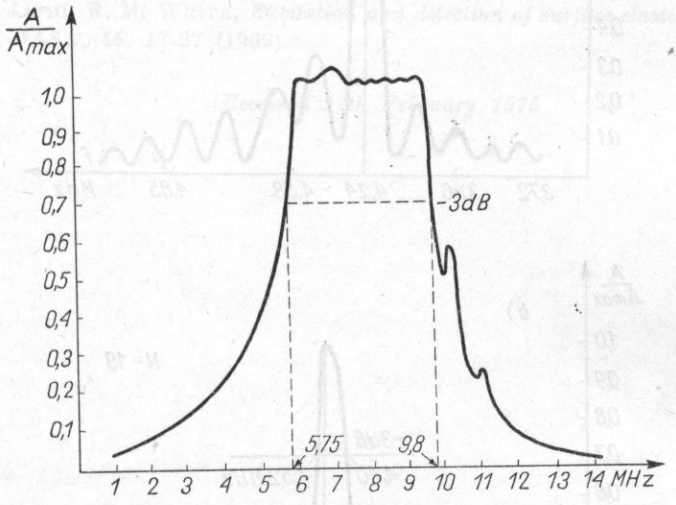

Fig. 5. The filter frequency characteristics

The transmitting transducers of the type $(\sin x)/x$ – the number of electrode pair $N = 19$. The simple receiving transducer – the number of electrode pair $N = 5$

The experimental investigations of the filters consisting of non-dispersive transducers with identically overlapping electrodes confirm the theoretical discussion with respect to their shape and frequency transmittance.

The characteristics were measured for transducers with the numbers of pair of electrodes $N = 11$, 19 and 23.

In spite of the fact that for 11 and 19 pairs of electrodes there is a discrepancy in certain frequency ranges between the characteristic measured and that assumed to be $A = (\sin a\omega)/(a\omega)$, the agreement between the theory and experiment for $N = 23$ is quite satisfactory.

As an example, we have presented the amplitude-frequency characteristics for 23 and 19 pairs of electrodes in non-dispersive transducers with constant overlapping electrodes.

The measurements of the characteristics show that the three-dimensional waves produced have not been attenuated.

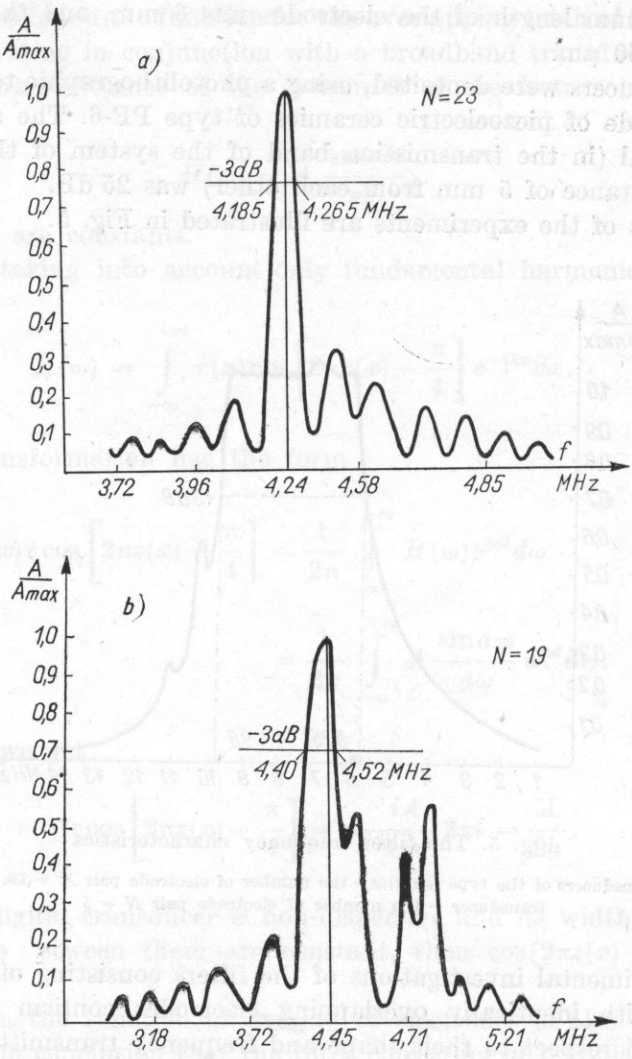

Fig. 6. The characteristics of a transducer system on a piezoelectric ceramic base

4. Conclusions

One of the factors responsible for the discrepancies between theory and experiment is the fact that only the fundamental harmonic has been considered. However, for a transducer with a greater number of electrodes, the contribution of higher odd harmonics in the frequency transmittance is low.

Thus it may be concluded that the method of determining the shape of electrode arrangement for an amplitude-frequency characteristic assumed a priori is convenient because of its simplicity, and the computing accuracy is satisfactory for numerous practical applications.

References

[1] R. H. TANCRELL, M. G. HOLLAND, *Acoustic surface wave filters*, Proceedings of the IEEE, **59**, 3 (1971).

[2] I. CERMAK, P. SYLVESTER, G. W. FARNELL, *Capacity and field distributions for interdigital surface wave transducers*, IEEE Trans. Son. Ultrason, 54-17 (1970).

[3] R. M. WHITE, *Surface elastic waves*, Proc. IEEE, 58 (1970).

[4] C. E. COOK, BERNFELD, *Radar signals*, Academic Press, New York 1967,

[5] W. D. SQUIRE, H. J. WHITEHOUSE, J. M. ALSUP, *Linear signal wave*, Theory Tech., vol. MTT-**17**, 1020-1040 (1969).

[6] S. G. JASHI, R. M. WHITE, *Excitation and detection of surface elastic waves in piezoelectric crystals*, JASA, **46**, 17-27 (1969).

Received 17th February 1975

ARCHIVES OF ACOUSTICS
1, 1, 43-50 (1976)

THERMAL RELAXATION PROCESSES IN SOME ORGANIC LIQUIDS

ZYGMUNT KLESZCZEWSKI

Institute of Physics, Silesian Technical University (Gliwice)

Measurements of propagation velocity and absorption coefficient of acoustic waves in some organic liquids have been made for frequencies between 10^6 Hz and 5×10^9 Hz at 20° C. On the basis of the data obtained the problem of thermal relaxation in liquids examined has been discussed. It was found that this process cannot be described by the relaxation time, which means that at a given frequency only some of internal degrees of freedom undergo excitation. Tests have been undertaken aimed at estimating which of the said degrees of freedom take an active part in the process of energy exchange.

Amongst many relaxation processes which occur during the propagation of an acoustic wave an essential role is played by that of thermal relaxation. While considering this process the assumption is very frequently made that it is characterized by one time of relaxation, which means that all external degrees of freedom undergo excitation simultaneously. This, however, is only a rough approximation.

In this paper, on the basis of the measurement of the propagation velocity of ultra- and hypersonic waves, the problem of thermal relaxation in some organic liquids will be discussed.

The following considerations will be true in the case when only one thermal relaxation occurs in the liquid.

It is assumed that the relaxation process is related to the energy exchange between the internal and external degrees of freedom. Assuming only one relaxation time it can be shown [2] that

$$\tau = \frac{2\alpha_\eta' v_0 c_p (c_v - c')}{c'(c_p - c_v)} \tag{1}$$

and

$$\left(\frac{v_\infty}{v_0}\right)^2 = \frac{\varkappa_\infty}{\varkappa_0}, \tag{2}$$

where τ means the time of relaxation, $\alpha_{\eta'}$ – absorption coefficient due to shear viscosity, v_0, v_∞ – velocities of acoustic wave, correspondingly to very low and very high frequencies,

$$\varkappa_\infty = \frac{c_p - c'}{c_v - c'}; \quad \varkappa_0 = \frac{c_p}{c_v},$$

c_p – molecular heat at constant pressure, c_v – molecular heat at constant volume, c' – molecular heat relative to internal degrees of freedom.

In addition, the relaxation time can be determined by experimental methods from measurements of the dispersion of the sound velocity. Namely [4]

$$\tau = \frac{A + (A^2 - 4\omega^2)^{1/2}}{2\omega^2}, \tag{3}$$

where $A = (\omega^2 \eta_0')/(v^2 - v_0^2)$, η_0' means static coefficient of volume viscosity, $\omega/2\pi$ – frequency of acoustic wave.

Measurements of the propagation velocity and absorption coefficient of hypersonic waves were made using the Mandelsztam-Brillouin dispersion effect. The measuring accuracy is 0.5%; absorption coefficient – approx. 20%. Within the ultrasonic range the measurements were made with the aid of an ultrasonic interferometer UI-10.

The results of measurements and calculations for the liquids examined are shown in Table 1. The $\varkappa_\infty/\varkappa_0$ values of specific heats necessary for the

Table 1. Calculated and measured values of the ratio v_∞/v_0 and relaxation times τ

Substance	c_p $\left[\frac{\text{J}}{\text{mol deg}}\right]$	c_v $\left[\frac{\text{J}}{\text{mol deg}}\right]$	c' $\left[\frac{\text{J}}{\text{mol deg}}\right]$	$\frac{\varkappa_\infty}{\varkappa_0}$	$\left(\frac{v_\infty}{v_0}\right)^2$	$\tau_0 \times 10^{10}$ [s]	$\tau_T \times 10^{10}$ [s]
Benzene	134.9	93.0	51.7	1.40	1.21	2.72	1.38
Carbon tetrachloride	129.0	87.1	49.7	1.42	1.24	0.78	0.57
Chloroform	83.8	77.5	32.7	1.25	1.09	2.27	0.61
Toluene	155.0	113.2	71.3	1.46	1.07	0.69	0.11
Methylene chloride	101.0	65.3	18.0	1.13	1.03	17.1	5.0
Methylene bromide	98.5	71.2	22.2	1.15	1.22	1.1	1.5
Chlorobenzene	161.3	118.0	66.6	1.33	1.12	0.68	0.26
Bromobenzene	155.2	117.2	64.5	1.30	1.10	0.84	0.14

calculation of this ratio are taken from [5]. Specific values of the internal degrees of freedom are evaluated from the formula

$$c_i' = d_i \frac{R\left(\frac{h\nu_i}{kT}\right)^2}{e^{\frac{h\nu_i}{kT}}\left(1 - e^{-\frac{h\nu_i}{kT}}\right)^2}, \tag{4}$$

where d_i means multiplication factor of degeneration at given frequency, ν_i — vibration frequency of degree i of freedom, R — gas constant, h — Planck constant, k — Boltzmann constant, T — absolute temperature.

Column 6 contains the experimental value of the ratio v_∞/v_0. In column 7 the relaxation time τ_0 as is given evaluated from the measurement of the dispersion of the sound velocity, while in column 8 the relaxation time τ_D calculated on the basis of formula (1). A considerable divergency between the times of relaxation τ_D and τ_T as well as the ratio $(v_\infty/v_0)^2$ and $\varkappa_\infty/\varkappa_0$ is evident.

Except for methylene bromide the experimental value v_∞/v_0 is in all cases smaller than the theoretical one. Hence, it can be concluded that within the examined frequency range of the acoustic wave only some of internal degrees of freedom participate in the energy exchange process with internal degrees of freedom or, to put it in another way, the relaxation times of various internal degrees of freedom are different.

It is expected that, first of all, the excitation affects the degrees of freedom with lowest frequency since the likelihood of their excitation is the highest. With very low frequency of acoustic wave the state of equilibrium is established. All internal degrees of freedom participate in the energy exchange process with external degrees of freedom. Namely, the time of equilibrium stabilization is shorter than the acoustic wave period. For higher frequencies of the acoustic wave the state of equilibrium can be achieved only for those external degrees of freedom, for which the time necessary to produce the oscillatory quantum and the time within which it is again transformed into the translating energy; thus the relaxation time is smaller than the acoustic wave period. This condition can be satisfied primarily for those internal degrees of freedom for which the least amount of energy for excitation is necessary, whereas the remaining degrees of freedom, if they undergo excitation at all, will not manage to transfer their energy into the translatory motional energy.

For higher acoustic wave frequencies the internal degrees of freedom, commencing from those for which the excitation energy is the largest, undergo «freezing», since the time necessary for their excitation is longer than the acoustic wave period. When the latter becomes very small, that is, when we go on to very high frequencies, all degrees of freedom undergo «freezing» and the specific heat of the substance is reduced. Having this in mind tests have been performed to ascertain which of degrees of freedom participate in the energy exchange process.

Thus, if v_∞ and v_0 are measured, c' can be evaluated from the formula

$$\left(\frac{v_\infty}{v_0}\right)^2 = \frac{(c_p - c')\,c_v}{(c_v - c')\,c_p},$$

c' will be designated in the following text as c_{ak}, since it can differ from the specific heat of internal degrees of freedom calculated from spectroscopic data.

The velocity v_0 measured at the frequency 10^6 Hz, the velocity v_∞ – at the frequency 5×10^9 Hz. Evaluating c_{ak} we have

$$c_{ak} = \frac{\left[1 - \left(\frac{v_0}{v_\infty}\right)^2\right] c_p}{\varkappa_0 - \frac{v_0^2}{v_\infty^2}}. \tag{5}$$

It can be seen from Table 2 that for all liquids except for methylene bromide the value of the molar heat calculated from spectroscopic data is higher than that of the molar heat obtained from acoustic measurements. It only supports the earlier suggestion that the relaxation times of various internal degrees of freedom are different, which means that at a given frequency of the hypersonic wave only some of the internal degrees of freedom participate in the process of energy exchange.

Table 2. Values of specific heats c_{ak} and c' for examined liquids

Substance	c_{ak} $\left[\frac{\text{J}}{\text{mol deg}}\right]$	c' $\left[\frac{\text{J}}{\text{mol deg}}\right]$
Benzene	37.5	51.7
Carbon tetrachloride	37.0	49.7
Chloroform	15.9	32.7
Toluene	23.1	71.3
Methylene chloride	11.3	18.0
Methylene bromide	27.2	22.2
Bromobenzene	33.5	64.5
Chlorobenzene	37.7	66.6
Nitrobenzene	37.7	65.7

To have more insight into the problem, let us consider in greater detail the vibration of molecules. Table 3 contains frequencies and corresponding specific heats of internal degrees of freedom of the benzene molecule. The values of vibration frequencies are taken in all cases from papers [1, 3].

The comparatively best agreement with experiment is obtained when vibrations belonging to the same class of symmetry are grouped. Vibrations ν_1, ν_3, ν_5, ν_7, ν_{10}, ν_{11}, ν_{14}, ν_{15}, ν_{16}, ν_{17}, and ν_{20} belong to the class type E. The value of specific heat of these internal degrees of freedom is 36.45 J/mol deg. Vibrations ν_2, ν_6, ν_9, ν_{12} and ν_{18} belong to the symmetry class type B, while vibrations ν_4, ν_8, ν_{13} and ν_{19} to the symmetry class type A. Corresponding values of specific heats are 9.95 J/mol deg and 5.57 J/mol deg, respectively.

If we assume that the calculated relaxation time $\tau = 2.7 \times 10^{-10}$ s is related to the excitation of vibrations belonging to the symmetry class type E, then the value $c_{ak} = 37.5$ J/mol deg is very close to that of the specific heat for these

Table 3. Values of vibration frequencies ν_i and specific heats c_i' of internal degrees of freedom for benzene

ν	$\nu_i \times 10^{-12}$ [s^{-1}]	d_i	c_i' $\left[\frac{J}{mol\,deg}\right]$	ν	$\nu_i \times 10^{-12}$ [s^{-1}]	d_i	c_i' $\left[\frac{J}{mol\,deg}\right]$
ν_1	12.11	2	12.24	ν_{11}	35.46	2	1.72
ν_2	15.08	1	5.15	ν_{12}	39.55	1	0.55
ν_3	18.17	2	8.38	ν_{13}	42.05	1	0.42
ν_4	20.19	1	3.61	ν_{14}	44.52	2	0.59
ν_5	20.74	2	6.54	ν_{15}	47.58	2	0.42
ν_6	23.45	1	2.77	ν_{16}	55.59	1	0.08
ν_7	25.56	2	4.61	ν_{17}	91.52	2	—
ν_8	29.78	1	1.55	ν_{18}	91.71	1	—
ν_9	30.09	1	1.47	ν_{19}	91.82	1	—
ν_{10}	31.07	2	2.68	ν_{20}	93.03	2	—

degrees of freedom. On the other hand the time of relaxation related to the excitation of vibrations belonging to the symmetry class types A and B differs greatly from the period of the hypersonic wave under consideration.

It is also possible to achieve a satisfactory agreement with experiment, if we assume that the relaxation time is related to the excitation of internal degrees of freedom with lowest frequencies: $\nu_1, \nu_2, \nu_3, \nu_4, \nu_5, \nu_6$. Specific heat of these internal degrees of freedom is 38.65 J/mol deg which is very close to $c_{ak} = 37.5$ J/mol deg. The remaining internal degrees of freedom with frequencies from ν_7 to ν_{20} at the given frequency of the acoustic wave do not undergo excitation since in this case a selective excitation of vibrations is encountered to which reference has already been made. The time required for their excitation is higher than the acoustic wave period.

Table 4. Values of vibration frequencies ν_i and specific heats c_i' of internal degrees of freedom for carbon tetrachloride

ν	$\nu_i \times 10^{-12}$ [s^{-1}]	d_i	c_i' $\left[\frac{J}{mol \times deg}\right]$
ν_1	6.54	2	15.10
ν_2	9.41	3	20.69
ν_3	13.75	1	5.52
ν_4	23.14	3	8.40

Table 4 contains frequencies and specific heats of internal degrees of freedom of carbon tetrachloride. The best agreement with the experimental value c_{ak} will be obtained if we assume that vibrations ν_2, ν_3 and ν_4 account for the relaxation processes within the examined frequency range.

The relaxation time connected with the excitation of the vibration ν_1 is considerable shorter. This seems to be justified, since the likelihood of the excitation of the vibration with lowest energy is the highest. Consequently, it very quickly undergoes excitation, while at the tested frequency of the hypersonic wave, $f = 4 \times 10^9\ s^{-1}$, transfer of energy to the internal degrees of freedom will occur and the state of equilibrium will be established. The value of the specific heat $c'_{2,3,4} = 34.61$ J/mol deg differs from c_{ak}, but it seems that such

a possibility is the most probable, particularly the case of CCl_4 where the Fermi resonance is likely to result, since $\nu_2+\nu_3 \simeq \nu_4$ and vibrations $\nu_2+\nu_3$ and ν_4 belong to the same symmetry class.

The situation is similar in the case of methylene chloride. Table 5 contains vibration frequencies of the of internal degrees of freedom and their specific heats.

Table 5. Values of vibration frequencies ν_i and of specific heats c_i' of internal degrees of freedom for methylene chloride

ν	$\nu_i \times 10^{-12}$ [s^{-1}]	d_i	c_i' $\left[\frac{J}{mol\,deg}\right]$
ν_1	8.50	1	7.13
ν_2	21.23	1	3.44
ν_3	22.18	1	3.18
ν_4	27.07	1	2.10
ν_5	34.62	1	1.05
ν_6	37.84	1	0.67
ν_7	42.99	1	0.42
ν_8	89.52	1	—
ν_9	90.03	1	—

Table 6. Values of vibration frequencies ν_i and specific heats c_i' of internal degrees of freedom for chloroform

ν	$\nu_i \times 10^{-12}$ [s^{-1}]	d_i	c_i' $\left[\frac{J}{mol\,deg}\right]$
ν_1	7.75	2	14.80
ν_2	11.09	1	6.41
ν_3	20.08	1	3.68
ν_4	22.81	2	6.05
ν_5	36.42	2	1.72
ν_6	90.01	1	—

If we assume that vibrations with the lowest frequency ν_1 participate in the energy exchange process with the external degrees of freedom, which means that their relaxation time is considerably shorter than the hypersonic wave period, then the specific heat of the remaining internal degrees of freedom is $c' = \sum_{i=2}^{9} c_i' = 10.86$ J/moldeg which is in satisfactory agreement with the value $c_{ak} = 11.3$ J/moldeg. Thus, the calculated relaxation time $\tau = 1.71 \times 10^9$s would be connected with these eight internal degrees of freedom.

Another possibility is that the above mentioned relaxation time is related to vibrations ν_1, ν_2, ν_7, and ν_8 which belong to the same symmetry class. The value of the specific heat $c_{1,2,7,8}'$ is 10.99 J/moldeg which is very close to the value c_{ak}.

From the foregoing it can be seen that it is not possible to determine unequivocally which of the internal degrees of freedom participates in the energy exchange process with external degrees of freedom during the propagation of an acoustic wave even though a suitable value of specific heat is obtained.

Even more complex is the problem in the case of chloroform for which the frequency of internal vibrational degrees of freedom and corresponding specific heats are stated in Table 6. This could be expected since the previously calculated values of the relaxation times from the half-width of spectral lines of dispersed light and from sound velocity dispersion differ greatly.

If we group vibrations in the same symmetry class, thus ν_1, ν_4, ν_5 as well as ν_2, ν_3 and ν_6, then the corresponding values of specific heats are respectively: $c'_{1,4,5} = 22.57$ J/moldeg and $c'_{2,3,6} = 10.09$ J/moldeg. However, if we assume that the calculated relaxation time $\tau = 2.27 \times 10^{-10}$ is related to the excitation of internal degrees of freedom from ν_2 to ν_6, then the value of specific heat $c'_{2,3,4,5,6}$ is 17.86 J/moldeg. Both this value and the previous ones differ essentially from the value of specific heat calculated from acoustic data, $c_{ak} = 15.9$ J/moldeg. It should be concluded that in the case of chloroform there occurs a superposition of several relaxation processes the times of which are only approximate.

Methylene bromide is the only one of the examined liquids for which $(v_\infty/v_0)^2 > \varkappa_\infty/\varkappa_0$, and this leads to the calculated c_{ak} being higher than c'. It should be concluded that in this case it is predominately other processes which cause an additional dispersion of sound velocity.

Because of a large number of internal degrees of freedom a very complex problem is encountered in the cases of chlorobenzene, bromobenzene and nitrobenzene. However, the data obtained permit the following conclusions pertaining to chlorobenzene to be derived. A good agreement with the experimental is achieved if one assumes that the relaxation time of the internal degrees of freedom with frequencies from 5.91×10^{12} s^{-1} to 9.17×10^{12} s^{-1} is shorter than $\tau = 0.84 \times 10^{-10}$s. This time would correspond to the excitation of internal degrees of freedom with frequencies from 20.02×10^{12} s^{-1} to 91.18×10^{12} s^{-1}.

Equally good agreement with the value c_{ak} is obtained on the assumption that the calculated relaxation time $\tau = 0.84 \times 10^{-10}$ s is connected with the excitation of vibrations from 5.91×10^{12} s^{-1} to 30.41×10^{12} s^{-1}. The specific heat corresponding to these internal degrees of freedom is 37.6 J/moldeg and this is in very good agreement with the value $c_{ak} = 37.7$ J/moldeg. The remaining internal degrees of freedom are no longer active in the energy exchange process with the external degrees of freedom.

The relaxation time of bromobenzene for the processes connected with the excitation of internal degrees of freedom with frequencies from 5.94×10^{12} s^{-1} to 10.79×10^{12} s^{-1} is shorter than 0.68×10^{-10} s whereas vibrations with frequencies from 18.38×10^{12} s^{-1} to 91.72×10^{12} s^{-1} account for the relaxation processes within the examined frequency range.

For nitrobenzene the best agreement with experiment is achieved on the assumption that the relaxation time of vibrations with frequencies varying from 5.27×10^{12} s^{-1} to 10.73×10^{12} s^{-1} is shorter than 0.5×10^{-10} s.

From the examples given it can be concluded that the process of thermal relaxation is complex and cannot be described by only one relaxation time. At a given frequency of the acoustic wave usually only some of the internal degrees of freedom participate in the energy exchange process. However it is not possible to prédict how this process will proceed.

References

[1] G. HERZBERG, *Infrared and Raman spectra of polyatomic molecules*, Princeton, New York 1945.

[2] K. HERZFELD, T. LITOVITZ, *Absorption and dispersion of ultrasonic waves*, Academic Press, New York 1959.

[3] LANDOLT – BÖRNSTEIN, *Zahlwerte und Funktionen aus Physik*, Chemie, Astronomie, Geophysik und Technik, **2** (1956).

[4] I. G. MICHAIŁOW, B. A. SAŁOWIEW, P. SYRNIKOW, *Fundamentals of molecular acoustics* [in Polish], Publ. «Nauka», Moskwa 1964, 235-282.

[5] J. TIMMERMANS, *Physic-chemical constants of pure organic compound*, New York 1957.

Received 13th June 1975

ARCHIVES OF ACOUSTICS
1, 1, 51-63 (1976)

ULTRASONIC HOLOGRAPHY IN OPHTHALMOLOGY — PHYSICAL CONSIDERATIONS*

ROBERT C. CHIVERS

Physics Department, University of Surrey, Guildford (Great Britain)

The characteristics of the ultrasonic holography unit under clinical trial in ophthalmic applications is discussed with particular emphasis on its advantages and limitations. Discussion of the factors influencing the quality of pictures in B-scanning and holography is also given.

1. Introduction

The ultrasonic A and B-scans have found continued application in ophthalmology since the pioneering work of OKSALA and LEHTINEN [15, 16] and BAUM and GREENWOOD [4], and although both methods of display have their advocates, the most effective diagnostic tool (as in obstetrics) is a combination of both, THIJSSEN [18]. The maximum potential of either technique is only achieved by experienced operators, and the temptation to collect and store information from three dimensions for subsequent retrieval and assessment by clinicians has proved irresistible.

Computing techniques, involving the collection and storage of serial A-scans or B-scans (e.g. MILAN [14]) are severely limited in ophthalmic applications because of the very high sampling rates required at the high frequencies (typically 8-15 MHz) used in diagnostic ophthalmic ultrasound, and also because of the great volume of data that has to be stored and processed. Compared to these difficulties, the analogue approach of holography appears at first sight to be favoured in application to the eye, which is accessible, has low attenuation coefficients (typically 0.1 dB/cm for the ocular media) and a regular anatomy in the normal. The bony protective socket in which the eye sits demands a reflection technique, since the transmission methods of holography favoured by investigators for other areas of the body (HOLBROOKE et al. [11] and METHERELL [13]) are rendered impotent by the variability in the attenuation of skull bone (CURRY et al. [8]).

---

* Paper presented at 21st Polish Open Seminar on Acoustics, Rzeszów, 1974.

As with all current forms of acoustical holography, the greatest problem is presented by the lack of a suitable acousto-optical converter or a means of recording the ultrasonic intensity distribution over an area of linear dimension much larger than the wavelength with a resolution of the order of a wavelength. The liquid surface levitation approach, while permitting real-time visualization is difficult to implement in a clinical situation for ophthalmic investigations. Apart from the multiplexing of B-scans (GREGUSS [9]), two solutions have been suggested to date.

The first of these (GREGUSS and BERTENYI [10]) used the interrogating beam from the transducer as the reference beam. The beam irradiating the eye passed through a sonosensitive plane that intercepted the reflected echoes, and, after development, provided the hologram. It would appear that the poor resolution and lack of easily-interpretable reconstructions has prevented continued use of this technique.

ALDRIDGE et al. [1] described in 1971 a pilot study with a system employing a mechanically-scanned transducer to sample over an aperture above an excised eye. Multiplication of the time-gated echoes from a region of the eye with an electronic reference related to the tone-burst exciting the transducer permitted the hologram to be constructed point by point on a facsimile recorder. Modification of the technique was required (ALDRIDGE et al. [2]) before it could be evaluated clinically. The philosophy of the prototype built for clinical use has been discussed fully elsewhere (ALDRIDGE et al. [2]). This paper discusses the demands of the clinical environment upon the development of the machine, indicates some of the difficulties associated with its use as a clinical tool and concludes with a discussion of the studies that will be necessary for its meaningful evaluation.

2. Machine-patient interface

The scanning mechanism built at the Atomic Energy Research Authority, Harwell provided a rectilinear scanning mode for the transducer over an area 4 cm square. The 10 MHz transducers used were sharply focussed at a distance of about 1 cm from the crystal face and the focal plane (because of instrumental requirements) needed to be about 2 cm above the eye being investigated (Fig. 1). In order to couple the transducer to the eye, some form of water bath was required. The open bath was used, consisting of a surgical drape filled with hyponormal Ringer's solution at 37 °C and supported by a square metal frame (Fig. 2). The assembly of the bath takes a skilled operator 5-10 minutes, but has the advantages over the closed type of bath (which is applied to the closed eyelid) of removing the acoustical complication of the membrane and coupling grease at the bottom of the closed bath, and allowing the eyelid to be open to obtain better penetration. The use of a single eye bath precludes the easy comparison of scans from one eye with those from the other, but in cases where

the free eye is sighted, it may be employed to keep the direction of gaze fixed (with a fixation light). The frame supporting the surgical drape is attached to a bar at the side of the bed, to enable it to be adjusted to the correct position over the patient's eye. The scanning area of the transducer is located with the aperture of the frame by suspending the transducer scanning movement from a gantry (Fig. 3), along which it may be moved. Adiustment is completed by movement of the patient's bed in a direction perpendicular to the gantry and

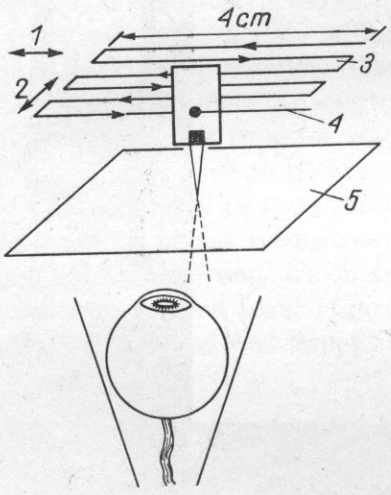

Fig. 1. Scanning geometry

1 – fast scanning, *2* – slow scanning, *3* – surface of scanning, *4* – transducer, *5* – focal surface

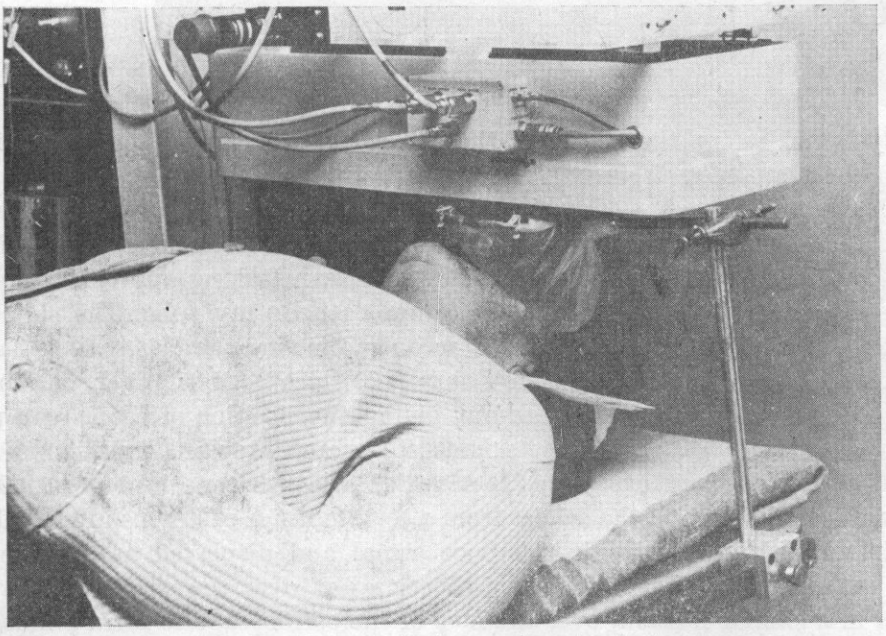

Fig. 2. Scanning mechanism and water bath on eye

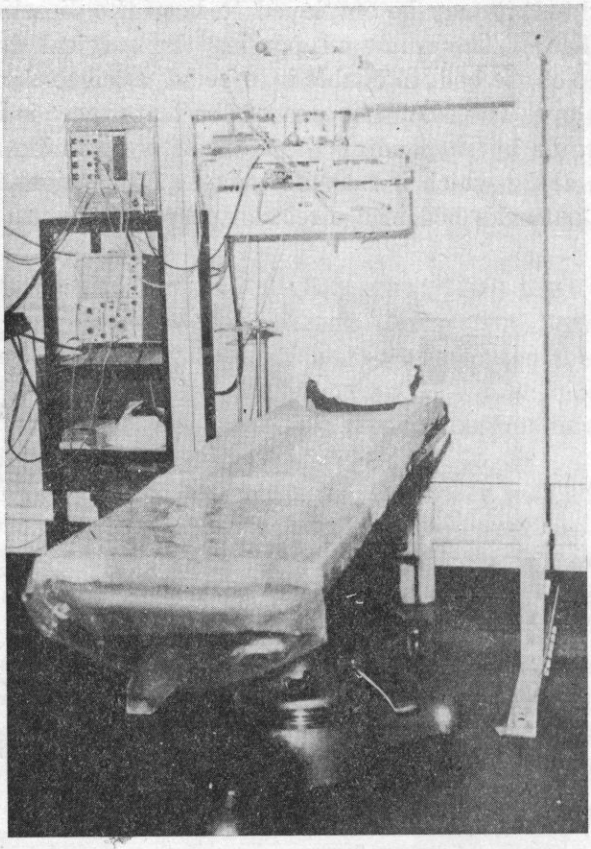

Fig. 3. Gantry and scanning mechanism

finally by adjusting the height of the bed (using a hydraulic pump) until the tip of the transducer is just in the water bath.

The scanning regime (described by ALDRIDGE et. al. [2]) consists of a fast linear scan in one dimension coupled with a slower scan in a perpendicular direction. With each 4 cm sweep of the fast scan (taking approximately 120 ms) a B-scan is produced on a non-storage cathode ray tube. The slow scan of 4 cm may take between 12 and 23 seconds allowing the fast scan to sample between 1/2 mm (80 lines) and 1/4 mm (160 lines). Alternatively it may be adjusted manually, a digital read-out giving the position of the B-scan plane displayed relative to an arbitrary origin with an accuracy of 1 mm.

The transducer is excited with a variable length tone burst of 10 MHz. To produce a hologram, the echoes from a certain range of depths are gated out, multiplied with an electronic reference signal and displayed as an intensity on a cathode ray tube. As the transducer scans over the aperture, the spot scans, in a similar fashion, over the face of the oscilloscope to form a hologram by being integrated onto a «Polaroid» negative film. Development of the film

takes only 3 minutes after which it may be reconstructed (prior to dismissal of the patient) on an optical bench in a darkroom adjacent to the examination room. The reconstruction may be viewed by eye, or displayed on a closed circuit television system, or recorded photographically.

3. Comparison of B-scanning and holography

The essence of the hologram produced, since it is not reconstructed in real time, is that it provides an easy and compact (it is essentially a slide 35 mm) method of storing ultrasonic information from a three-dimensional volume of soft tissue. The volume of tissue is defined by the limits of the aperture scanned, the delay before the acceptance time gate opens, the time for which the gate is open and the length of the pulse of ultrasound used to obtain the hologram. It is only possible to display a single plane (parallel to the scanning plane) from this volume at any one time. However the planes reconstructed are inaccessible to any B-scan (because of the orbital wall) and are in fact perpendicular to those of the B-scans displayed from the fast-scan. Figure 4 shows the B-scan of an excised eye (the long pulse length used was responsible

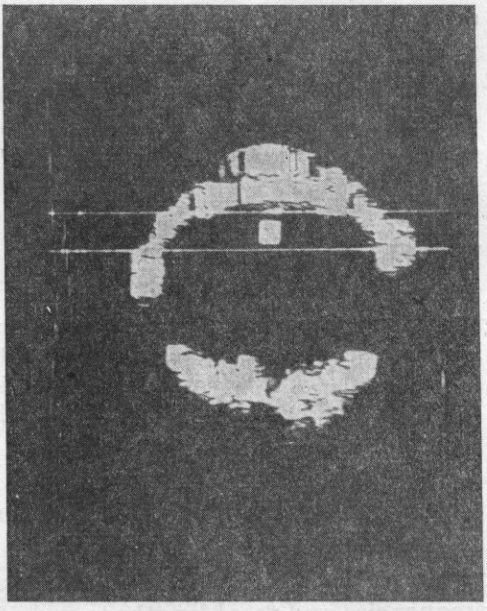

Fig. 4. B-scan of excised eye. The poor resolution is caused by the use of a long pulse length

for the poor resolution). The two white lines indicate the limits of the acceptance gate for making a hologram. A reconstruction of the hologram is shown in Fig. 5, where the circular nature of the cross-section of the eye can be clearly

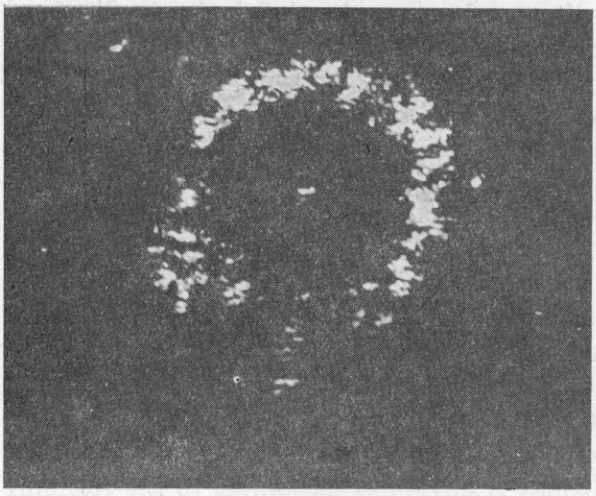

Fig. 5. Reconstruction of hologram taken of the volume between the horizontal lines representing the acceptance gate on Fig. 4

seen, as can the back of the lens (appearing as a bright spot in the centre). The ragged nature of the outer ring is due to attached tissue.

ALDRIDGE et al. [2] using targets with simple geometry have shown the lateral resolution of the hologram to be of the order of 0.5 mm and the depth resolution to be approximately 5 mm. The depth resolution of the B-scan depends entirely on the pulse length which may be varied down to 0.5 μs ($\simeq 0.3$ mm of tissue for a pulse-echo system); while the lateral resolution depends on the focussing properties of the transducer. Consideration of the means of optimizing the two different displays shows that they present conflicting requirements, as summarized in Table 1 (CHIVERS [7]). The B-scan requires

Table 1. Parameters for optimizing displays

	Pulse length	Transducer	
		focal length	focus
B-scan	Short for good resolution	Medium (chosen for region of interest)	Weak
Holography	Long for good signal to noise ratio	Short	Sharp for good resolution

a weakly focussed transducer that has its minimum beam width in the region of diagnostic interest, and should be excited by a very short pulse. Ideally a range of transducers should be available (BUSCHMANN [6]) with different frequencies and focal lengths to provide the optimum display for a clinical condition. The hologram, on the other hand, requires a very sharp focus (the focal spot size determines the lateral resolution) close to the transducer. In addition to this, increasing the length of the pulse used to excite the transducer generally increases the signal to noise ratio of the hologram.

4. B-scanning

The value of a linear B-scan is limited severely in ophthalmic applications by the adverse geometry of the anatomy of the eye, with the convex refracting surfaces it presents to the interrogating sound beam (Sokollu [17]). The limitations are even more severe if unfavourably focussed transducers are used. Nevertheless, the B-scan incorporated into the holographic system has several uses. Its main use is to provide a visual monitor of the position of the hologram gate, permitting its quick and confident adjustment (see Fig. 4).

As a diagnostic tool in its own right it has the usual (and necessary) variable gain and swept gain. In addition to these, the display includes a compression amplifier to display «grey-scale» pictures of the orbital fat, and a variable pulse length. The diagnostic trials in progress are aimed at determining the optimum use of these four mutually dependent parameters that effect the display. Figure 6 shows the effects of a) high gain and low swept gain, b) low gain and high swept gain, and c) low gain and low swept gain with compression for a particular (short) pulse length.

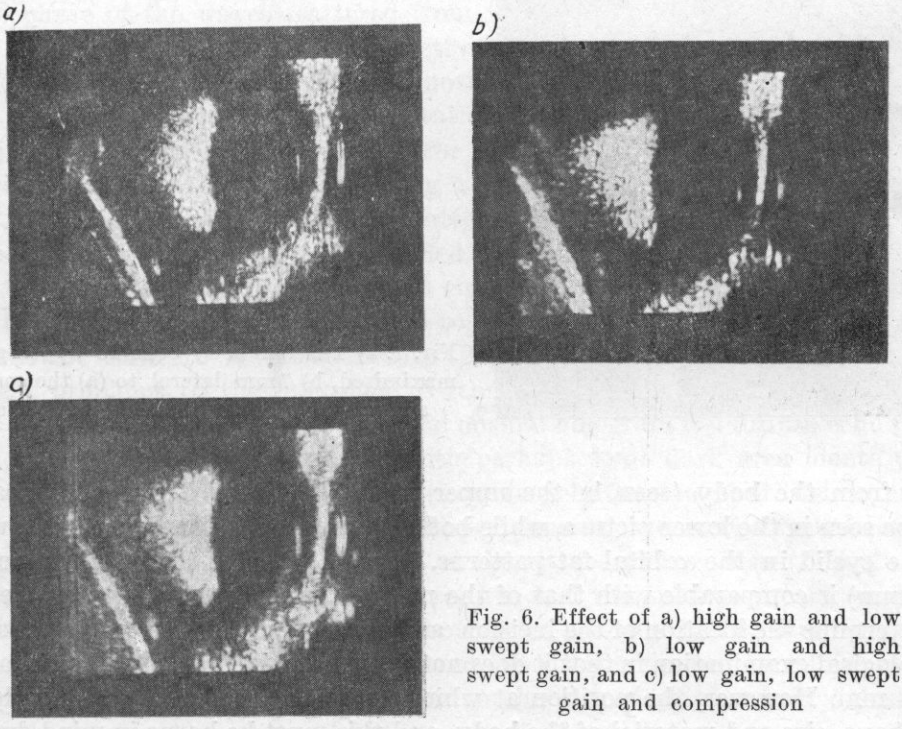

Fig. 6. Effect of a) high gain and low swept gain, b) low gain and high swept gain, and c) low gain, low swept gain and compression

The clinical value of the B-scan has yet to be assessed, although preliminary results with detached retinas, ocular and orbital tumours and intra-ocular

foreign bodies are encouraging. The fast nature of the scan makes it an almost real-time display that can be used with advantage in dynamic studies. Figure 7 illustrates the value of the scan in the localization of a foreign body. The scanning mechanism has been rotated through 90° to permit the fast scan to run from head to toe of the patient. Manual adjustment of the slow scan enables the echoes from the cornea and front of the lens to be maximized (lower picture). The reading on the slow-scan position scale is taken as the reference to be subtracted from the reading at the position corresponding to the maximum

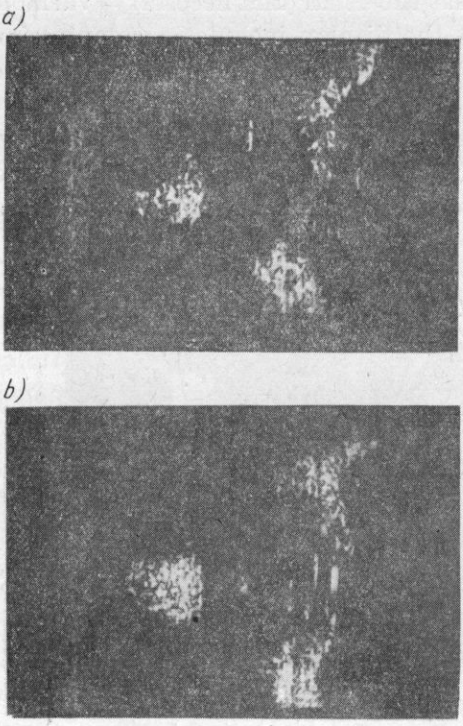

Fig. 7. a) Foreign body echo in upper globe maximized, b) 7 mm lateral to (a) the corneal and anterior lens echoes are maximized

echo from the body (seen in the upper picture). Some vitreous disturbance can be seen in the lower picture, while both pictures show clearly the shadowing of the eyelid in the orbital fat patterns. The accuracy of this localization (to < 1 mm) is comparable with that of the methods used in the operating theatre to determine the location of the incision, and has the advantage over the normal radiological examination in that it does not depend on an average globe diameter of 24 mm. However, the position at which the echo is maximized depends on the shape, size and material of the body, and this must be borne in mind during the investigation. In particular, a negative result does not exclude the existence of a foreign body (an unfavourably orientated air-gun pellet, for example, reflects almost no echoes to a linearly scanned transducer).

5. Holography

The figures of the resolution specified earlier were obtained using targets of known simple geometry, with a greater acoustic mismatch to their surroundings than is represented by an element of soft tissue in the eye. They therefore represent the optimum rather than the norm that might be expected in a clinical situation. There are two elements in the assessment of clinical holograms: firstly the signal to noise ratio, and secondly the interpretation of the patterns in the reconstruction.

Four factors can contribute noise to the hologram reconstruction:

1. dust or scratches on the hologram itself — these may be minimized with careful handling,

2. movement of the eye during the scan — sometimes the patient's eye follows the movement of the scanning mechanism in the slow-scan direction. This can be minimized with a fixation light for those patients with binocular vision, but blinking or similar muscular contractions may degrade the information content of the hologram,

3. the effect of paths through different tissues (particularly the lens) on the phase of the waves scattered from a certain depth,

4. information from planes in the hologram volume, other than the one that is in focus (and thus being reconstructed).

The maximum signal to noise ratio is thus achieved by using long pulses, using the maximum sampling rate for the fast scan consistent with the transducer focal spot size, and by taking a hologram of only a thin slice.

In the globe, the problem of pattern recognition is relatively simple since the normal is a black circle surrounded by a white ring of tissue, and any signal in the circle suggests a pathological condition. One advantage of the hologram is the visualization of regions close to the lateral walls of the globe, that are relatively hard to investigate with B-scans (although they do not present great problems to the hand-held A-scan).

In the orbit, as with B-scans, the normal hologram is a diffuse echo pattern of apparently random intensity (with perhaps some dark area identifiable as the optic nerve). Regions of foreign tissue may be detected, but their interpretation will need some care as their appearance on the reconstructed hologram will depend upon both the nature of the tissues above them (through which the sound pulse had to travel and return) and the tissues on each side of the reconstructed plane (that are contributing out-of-focus information). In addition to this the holograms can be affected by shadowing and multiple reflection artefacts, although careful attention to the B-scan display may detect these last.

Figures 8, 9 and 10 are reconstructions of holograms taken using stranded targets as a preliminary investigation of the significance of some of these effects. Figures 8 and 9 are reconstructions of a target of parallel nylon lines of 1/8 mm

diameter, spaced by 2 mm. Two centimetres above these an acrylic lens implant was supported by three lines of the same nylon thread. In both figures the black image of the lens implant can be seen. It is thought that this is a reflection artefact caused by the strong reflecting characteristic of the plastic compared to that of its supporting nylon strands which cannot be detected in the image

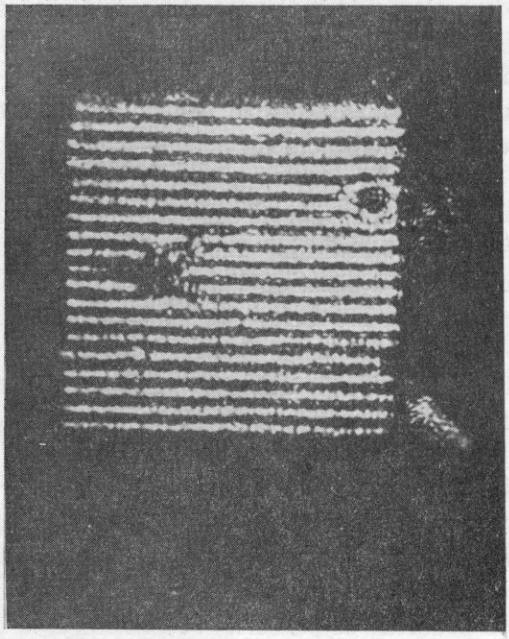

Fig. 8. Reconstruction of nylon thread target (thickness 1/8 mm, spacing 2 mm) with acrylic lens implant suspended 2 cm above. The black circle is caused by a small air bubble on the line supporting the lens implant

plane. In the top right hand section of Fig. 8 the effect of a small air bubble on the nylon supporting the lens implant can be seen. As expected, this appears as a dark patch with distortion of the pattern of the threads that are being visualized underneath it. This is the effect that might be anticipated from a small bubble of air caught for example in the eyelashes of a patient. Figure 9 shows the same target but with a small air bubble actually on one of its wires. This has less distorting effect than the bubble in Figure 8, but produces an (expected) strong highlight.

Figure 10 is the reconstruction of a freshly excised human anterior chamber with some attached tissue suspended 2 cm above a grid of parallel copper wires of 1/8 mm diameter spaced by 1.5 mm and is very much more disturbing. The extremity of the tissue appears to be matched by a thin dark line on the right-hand side of the picture. Immediately to the left of the line the pattern appears to be only minimally distorted, but it appears that in the centre or

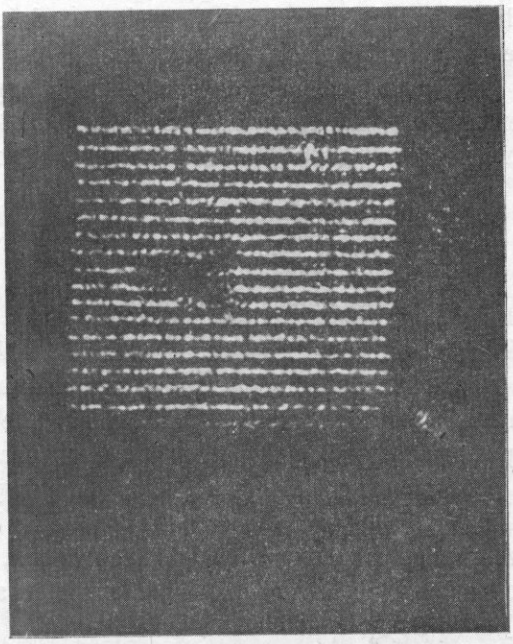

Fig. 9. As Fig. 7, but with air bubble actually on one of the threads being visualized (second from top)

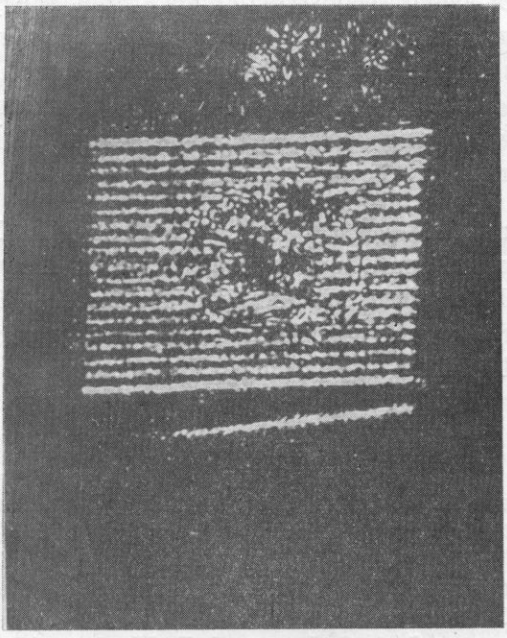

Fig. 10. Reconstruction of copper wire target (thickness 1/8 mm, spacing 1.5 mm) with freshly excised anterior chamber supported 2 cm above

where there is any thickness of tissue the pattern is completely lost. The darkest patch in the centre may represent a shadow caused by a relatively strong reflection from the lens, but the effect of the surrounding tissue is salutary. The relation between this picture and that reported by BOLDREY et al. [5] is not yet clear. The brightening effect of the lens that they report may be a diffraction phenomenon.

6. Conclusion

The characteristics of the ultrasonic holography unit under clinical trial at Moorfields Eye Hospital, London have been discussed with particular emphasis on the physical limitations of the linear B-scan and holographic displays it provides. The clinical trials in progress are aimed, for the B-scan, at defining the relative roles of gain, swept gain, pulse length and compression characteristics for different clinical conditions; and for the holographic display of assessing its potential and limitations as a new diagnostic method. The latter require assessment not only in relation to existing ultrasonic techniques, but also in relation to other methods of orbital examination. This work is already in progress (AMBROSE et al. [3]).

In addition to this, further laboratory studies are needed to assist in the interpretation of the diffuse orbital fat echo patterns and the effect of the overlying tissue upon them. The degradation of the signal to noise ratio by planes in the hologram not being reconstructed may limit the practical use of the system to the visualization of thin slices rather than substantial volumes. The relative merits of the holographic system compared to a simple C-scan (e.g. MCCREADY and HILL [12]) will then need evaluation.

The answers to these questions will evolve from the clinical trials in progress which will be reported subsequently.

Acknowledgment. The author wishes to thank Miss M. RESTORI for her assistance in the experimentation, his colleagues at Moorfields Eye Hospital and AERE, Harwell for their co-operation, the Medical Research Council for financial support for this work, and the IPC Press Ltd for permission to reproduce Figures 2, 3, 4 and 6, from the journal «Ultrasonics».

References

[1] E. E. ALDRIDGE, A. B. CLARE, G. A. S. LLOYD, D. A. SHEPHERD, J. E. WRIGHT, *A preliminary investigation of the use of ultrasonic holography in ophthalmology*, Brit. J. Radiol., **44**, 126 (1971).

[2] E. E. ALDRIDGE, A. B. CLARE, D. A. SHEPHERD, *Scanned ultrasonic holography for ophthalmic diagnosis*, Ultrasonics, **12**, 155 (1974).

[3] J. A. E. AMBROSE, G. A. S. LLOYD, J. E. WRIGHT, *A preliminary evaluation of fine matrix computerized axial tomography (Emiscan) in the diagnosis of space occupying lesions*, Brit. J. Radiol., **47**, 747-751 (1974).

[4] G. Baum and I. Greenwood, *The application of ultrasonic locating techniques to ophthalomology*, AMA Arch. Ophth., **60**, 263-279 (1958).

[5] E. E. Boldrey, D. R. Holbrooke, V. Richards, *Ultrasonic transmission holography of the eye*, Investigative Ophthalmology, **14**, 72-75 (1975).

[6] W. H. Buschmann, *Reproducible calibrations: the basis of ultrasonic differential diagnosis in A-mode and B-mode examination of the eye and orbit.* In *Ultrasonography in Ophthalmology* (Edited by M. A. Wainstock). Int. Ophth. Clinics, **9**, (3), 761-792 (1969).

[7] R. C. Chivers, *B-scanning and holography in ophthalmology*, Ultrasonics, **12**, 209-213 (1974).

[8] G. R. Curry, R. J. Stevenson, D. N. White, *The orbit and superior orbital fissure as an acoustic window*, Medical and Biological Eng., **11**, 293 (1973).

[9] P. Greguss, *Non-electromagnetic holography and its impact on biomedical research and clinical practice*, Acta Biochim. et Biopchys. Acad. Sci. Hung., **7**, 263 (1972).

[10] P. Greguss, A. Bertenyi, *Ultrasonic holography in ophthalmology*. In *Ophthalmic Ultrasound* (Edited by K. A. Gitter et al.), p. 81-4, C. V. Mosby, St. Louis 1969.

[11] D. R. Holbrooke, E. M. McCurry, V. Richards, H. R. Shibata, *Through transmission ultrasonic imaging of intrauterine and foetal structures using acoustical holography*. In *Ultrasonics in Medicine* (Edited by M. de Vlieger et al.), p. 332-344, Elsevier, New York 1974.

[12] V. R. McCready, C. R. Hill, *A constant depth ultrasonic scanner*, Brit. J. Radiol., **44**, 747 (1971).

[13] A. F. Metherell, *An acoustical holography medical imaging system using an optical detection and recording technique*. In *Ultrasonics in Medicine* (Edited by M. de Vlieger et al.), p. 55-66, Elsevier, New York 1974.

[14] J. Milan, *An improved ultrasonic scanning system employing a small digital computer*, Brit. J. Radiol., **45**, 911 (1972).

[15] A. Oksala, A. Lehtinen, *Diagnostics of detachment of the retina by means of ultrasound*, Acta Ophth., **35**, 461-467 (1957).

[16] A. Oksala, A. Lehtinen, *Über die diagnostische Vervendung von Ultraschall in der Augenheilkunde*, Ophthalmologica, **134**, 387-395 (1957).

[17] A. Sokollu, *Concise physics of ultrasound as applied in ophthalmology*. In *Ultrasonography in Ophthalmology* (Edited by M. A. Wainstock), Int. Ophthal. Clinics, 9, (3), 793-828 (1969).

[18] J. M. Thijssen, *Echo-ophthalmology: physical principles and diagnostic value*. In *Photography, Electro-ophthalmology and Echo-ophthalmology in Ophthalmic Practice* (Edited by H. E. Henkes), p. 273-318. Dr. W. Junk b. v. publishers, The Hague, Netherlands 1973.

Received 9th June 1975

ARCHIVES OF ACOUSTICS
1, 1, 65-71 (1976)

MEASUREMENTS OF ULTRASONIC VELOCITY IN THE MOLTEN SALT MIXTURE $CdCl_2$-NaCl

BRONISŁAW ZAPIÓR, ADAM JUSZKIEWICZ, ANDRZEJ GRZEGORCZYK

Institute of Chemistry, Jagiellonian University (Kraków)

The measurement of the ultrasonic velocity was carried out for the molten salt mixture $CdCl_2$-NaCl, in mole fraction ratios, for the temperature range 580-880°C. The adiabatic compressibility was calculated for each concentration at the temperature 680°C. The isothermal velocity and excess velocity as functions of the mole fraction have been illustrated for the temperature 840°C.

1. Introduction

Measurements of ultrasonic velocity in molten salt systems carried out simultaneously with density measurements are the basic source of data necessary to calculate the adiabatic compressibility β_s of such systems. Interpretation of adiabatic compressibility in terms of its relation to ion-ion interactions leads to a direct conclusion about the microscopic structure of the molten electrolytes. Most of the ultrasonic velocity measurements have been carried out for simple molten electrolytes [1, 2]. A consequence of these investigations has been the equation of state for simple molten electrolytes established by BOCKRIS. On the basis of scaled particle theory the sum of anion-cation radia for molten alkali halides has been calculated by STILLINGER Jr.

Investigations of some binary molten electrolyte mixtures have been carried out by STERNBERG and VASILESCU [3, 4]. These authors suggest the formation of ionic complexes of the type $PbCl_3^-$, $PbCl_4^{2-}$, $PbCl_6^{4-}$, in the investigated samples. It also seems possible that similar complexes could be formed in the molten binary mixture of $CdCl_2$-NaCl.

The results of our investigations reveal some evidence for the complexing of Cd^{2+} by Cl^- ions to form $CdCl_4^{2-}$ in the molten mixture $CdCl_2$-NaCl.

2. Experimental

Apparatus. The measurements of the ultrasonic velocity were carried out using an apparatus constructed in the General Chemistry Department of the Institute of Chemistry, Jagiellonian University.

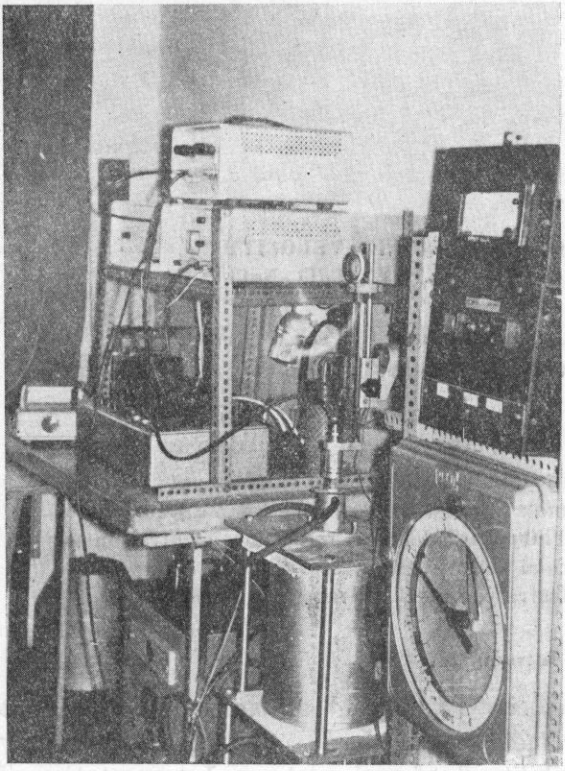

Fig. 1. General view of the apparatus for the measurement of ultrasonic velocity at high temperature

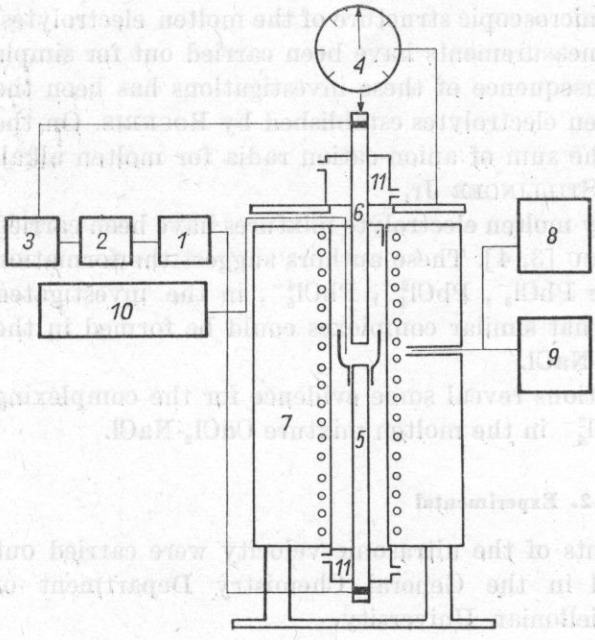

Fig. 2. Scheme of the apparatus for the measurement of ultrasonic velocity in molten salt systems

The apparatus was used to measure the velocity of ultrasound in molten salts, glass phases and alloys over the temperature range 100°-1000°C at two different ultrasonic frequencies, 5 and 10 MHz. Using a special micro-balance with a density bob, the density of a sample could be determined.

The apparatus consists of an ultrasonic generator *1*, amplifier with attenuator *3*, receiver *2*, support with a cathetometer for measuring the distance between the quartz rods with an accuracy of 10^{-5} m *4*, the vessel with the quartz delay rod and the transducer *5*, the transducing receiver with the quartz delay rod *6*, resistance oven *7*, thermal regulator *8*, temperature recorder 9, cooling coils *11* and a measurement assembly including a compensatory Wheatstone bridge *10*.

Table 1. Coefficients a and u_0 calculated from our results and compared with the results obtained by Vasilescu and Bockris

	Our results		Bockris		Vasilescu	
	a	u_0	a	u_0	a	u_0
NaCl	0.814	2402	0.915	2483	0.811	2405
$CdCl_2$	0.348	1272	0.382	1280	—	—

The electronic assembly included an ultrasonic pulse-phase UI-11 interferometer produced in Poland (IPPT PAN, Warsaw). Measurement of the ultrasonic velocity is based on the observed interference of two electrical pulses introduced simultaneously into the input of the receiver, one having passed through the ultrasonic transducers and the investigated sample, and the second

Table 2. The experimental temperature ranges for different samples

k_{mole}NaCl	Temperature range [°C]
0	580-890
0.1	580-860
0.2	600-870
0.3	610-860
0.4	500-860
0.5	600-870
0.6	580-880
0.7	640-870
0.8	630-880
0.9	755-880
1.0	above 807;

coming directly. The change of distance between the ultrasonic transducers causes a change in the resultant amplitude of the two pulses. Using the cathetometer we can measure the distance between two points having the same ampli-

tude (usually zero) for the same frequency f of the ultrasound; the velocity u can be derived from the following relationship

$$u = \Delta l f, \tag{1}$$

where Δl is the distance between the transducers.

Calibration of the apparatus. The standardizing measurements for the velocity of ultrasound were carried out in molten NaCl, temperature range 810°-920°C, and molten $CdCl_2$, temperature range 580°-880°C, at a frequency of 5 MHz. «Analar» materials were used for these measurements. The measured ultrasonic velocities in the above temperature ranges can be represented by the linear relationship

$$u = u_0 - at. \tag{2}$$

The coefficients u_0 and a, calculated from the above equation, are collected together in Table 1. Looking at this table we can compare the results for u_0 and a previously found by VASILESCU [3], BOCKRIS [1]. As can be seen from Table 1, the results are in good agreement and the error does not exceed 1.5 %.

Procedure. Measurements of the ultrasonic velocity were carried out for the mixture $NaCl/CdCl_2$ in different molar ratios. In Table 2 the temperature ranges for the different compositions are shown. The measurements were carried out three times for each sample, and the results, as a function of temperature and composition, are presented in Fig. 3.

As can be seen from Fig. 3 the relationship between the ultrasonic velocity and the temperature is linear for the whole sample range. The coefficient a changes with mixture composition from which we conclude that the investigated samples are not ideal liquids and that the observed deviations are due to the production of ionic complexes in solution.

This assumption is confirmed by the isothermal plot of ultrasonic velocity vs. mole fraction for 840°C (Fig. 4), where a negative deviation may be seen between the measured ultrasonic velocity and the additive velocities. The highest difference occurs for the mixtures 0.6 and 0.7 k_{mole} NaCl.

The excess velocity of the ultrasound u^E (Fig. 5) is calculated from the equation

$$u^E = u - u_1^0 k_1 - u_2^0 k_2 \tag{3}$$

(where u is the velocity in the mixture, and $u_1^0 k_1$ and $u_2^0 k_2$ are the velocities and molar fractions of the first and the second component of mixture, respectively) and has a minimum for the concentration 0.6-0.7, as was found above.

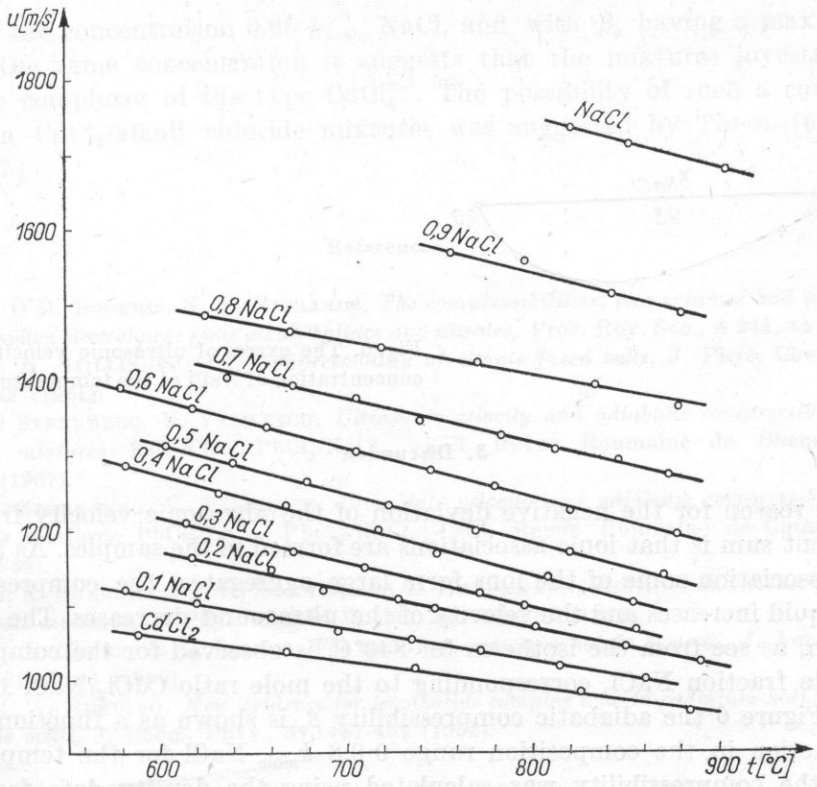

Fig. 3. Ultrasonic velocity vs. temperature in liquid mixtures of $NaCl/CdCl_2$

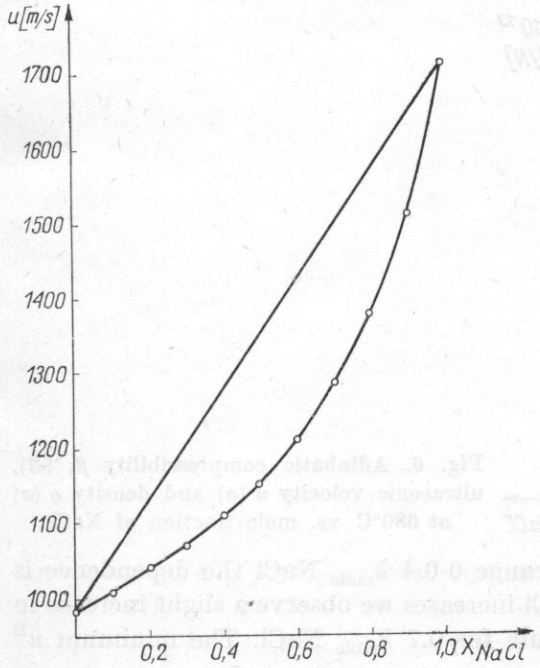

Fig. 4. Plot of ultrasonic velocity vs. mole fraction of NaCl at 840°C

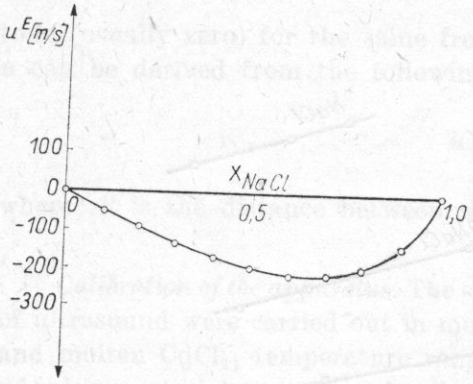

Fig. 5. The excess of ultrasonic velocity u^E vs. concentration of NaCl at the temperature 840°C

3. Discussion

The reason for the negative deviation of the ultrasonic velocity from the component sum is that ionic associations are formed in the samples. As a result of the association some of the ions form large aggregates, the compressibility of the liquid increases and the velocity of the ultrasound decreases. The highest deviation, as see from the isotherm for 840°C, is observed for the composition 0.66 mole fraction NaCl, corresponding to the mole ratio $CdCl_2$/NaCl 1:2.

In Figure 6 the adiabatic compressibility β_s is shown as a function of the mole fraction in the composition range 0-0.8 k_{mole} NaCl for the temperature 680°C; the compressibility was calculated using the density data found by

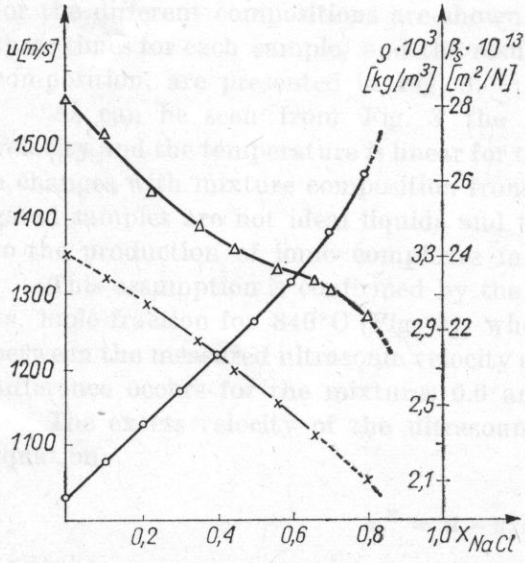

Fig. 6. Adiabatic compressibility β_s (Δ), ultrasonic velocity u (o) and density ϱ (x) at 680°C vs. mole fraction of NaCl

Heymann [5]. In the concentration range 0-0.4 k_{mole} NaCl the dependence is linear, but as the concentration of NaCl increases we observe a slight increase in compressibility up to a small maximum for 0.7 k_{mole} NaCl. The minimum u^E

occurs for the concentration 0.66 k_{mole} NaCl, and with β_s having a maximum value at the same concentration it suggests that the mixtures investigated form ionic complexes of the type $CdCl_4^{2-}$. The possibility of such a complex existing in $CdCl_2$/alkali chloride mixtures was suggested by TOPOL [6] and BREDIG [7].

References

[1] I. O'M. BOCKRIS, N. E. RICHARDS, *The compressibilities, free volumes and equation of state for molten electrolytes: some alkali halides and nitrates*, Proc. Roy. Soc., **A 241**, 44 (1957).

[2] F. H. STILLINGER, Jr., *Compressibility of simple fused salts*, J. Phys. Chem., **35**, 5, 1581-1583 (1961).

[3] S. STERNBERG, V. VASILESCU, *Ultrasonic velocity and adiabatic compressibility in molten salt mixtures*: KCl-KBr, $PbCl_2$-$NaCl_2$, -KCl, Revue Roumaine de Chemie, **12**, 1187-1197 (1967).

[4] S. STERNBERG, V. VASILESCU, *Ultrasonic velocity and adiabatic compressibility in molten salts mixtures*: $PbCl_2$-$LiCl_2$, $PbCl_2$-RbCl, -CsCl, Revue Roumaine de Chimie, **13**, 265-273 (1968).

[5] N. K. BOARDMAN, F. H. DORMAN and E. HEYNEMANN, *Densities and molar volumes of molten salt mixtures*, J. Phys. Colloid Chem., **53**, 375-382 (1948).

[6] L. E. TOPOL, A. L. LANDIS, *The cadmium-cadmium halide systems*, J. Am. Chem. Soc., **82**, 6291-6293 (1960).

[7] M. A. BREDING, *New evidence for tetrahalide complex ions in cadmium halide-alkali metal halide melts*, J. Chem. Phys., **37**, 451-462 (1962).

Received 7th May 1975

ARCHIVES OF ACOUSTICS
1, 1, 73-79 (1976)

ANALOGUE MODULATOR FOR PSYCHOACOUSTICAL PULSE MEASUREMENTS

ANTONI JAROSZEWSKI, ANDRZEJ RAKOWSKI

Laboratory of Musical Acoustics, Academy of Music (Warsaw)

A general description and some diagrams of the three channel analogue modulator are given. Some more important details of the construction are discussed.

1. Introduction

In present day methods of psychoacoustical measurements, simple continuous signals often undergo processing in the time and amplitude domains to deliver the required time paradigms of pulses with suitable envelopes. Such pulse signals are commonly used in research pertaining to the perception of pitch, loudness, timbre, to direct and residual masking, to short term and long term memory, to localization of sound sources etc., to name only a few examples.

Periodically repeated paradigms of pulse signals are used frequently if the method of adjustments is applied in the measurements. In such a case the subjects have means to adjust the specified parameter in one of signals presented (variable), so as to match the corresponding sensation to the sensation developed by the standard signal. Often in such paradigms masking or disturbing signals are added to the standard and variable signals.

Stimuli of various types are used in the measurements i.e. sine signals, harmonic and inharmonic multitones, stochastic signals, such as white and filtered noise, various frequency or amplitude modulated signals, etc. Sometimes, periodic signals with a composite spectrum are also used in the form of suitable pulse trains. These incoming signals are usually continuous functions of time.

With respect to signal timing in these methods, operational times in the region from 10^{-4} up to 10^{2} s are most commonly used. This refers both to the duty times of the stimuli and to the time intervals between them. Amplitude or envelope processing should transform the rectangular signal pulses into pulses with the required envelope shape. Gaussian function or linear functions are used most often for pulse shaping, but $\sin^2$, cos or other simple functions are also used. It is necessary that the parameters of the envelope are adjustable. In

general it means that the rise and decay slopes may be regulated. With linear functions the rise/decay slope is determined directly, whereas in case of Gaussian function it is expressed as the so-called «fuzziness» coefficient. With some other functions, e.g. $\sin^2$ and cos, it can be determined as a ratio of time intervals of the shaped fraction of the envelope to the whole duty time interval. It also is desirable that for each of the pulses in the paradigm, a different time-amplitude pattern can be chosen. In other words for each of the pulses in the paradigm a separate channel should be used for independent timing and envelope shaping. The number of separate pulses in the paradigms used in the majority of methods described is not greater than three.

2. General description

To meet the requirements discussed, a three channel analogue modulator has been designed. A block diagram of this modulator is given in Fig. 1.

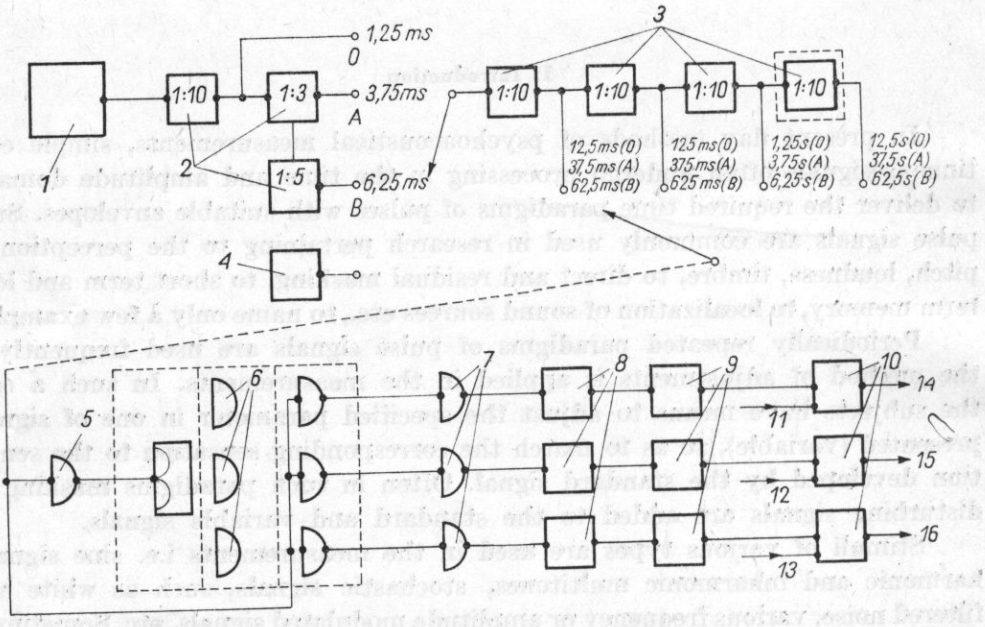

Fig. 1. Block diagram of the three channel analogue modulator

1 – quartz oscillator 8 kHz, *2*, *3* – frequency deviders, *4* – blocking oscillator, *5* – inverter, *6* – decoders, *7* – inverters, *8* – duty cycle adjustment circuits, *9* – rise/decay adjustment circuits, *10* – analogue gates, *11* – I signal input, *12* – II signal input, *13* – III signal input, *14* – I signal output, *15* – II signal output, *16* – III signal output

Three separate analogue gate circuits are used to perform the necessary processing of continuous signals into suitable pulses. The incoming continuous signals delivered to the inputs of these analogue gates obtain from them the required duty time, the suitable time location, and the envelope shape according to the chosen function.

Analogue gate circuits transmit the incoming continuous signals delivered to the inputs only in the presence of a keying signal. Thus, onset and cessation of the keying signal determine the onset and cessation of the incoming continuous signal, whereas the shape of the keying signal fix the shape of the envelope. Stimuli in the form of continuous signals thus processed constitute the required sequence of pulses (paradigm) which can be repeated over and over depending on the conditions of the experiment.

3. Timer

Keying signals are delivered from a quartz clock which consists of a conventional quartz stabilized oscillator operating at 8 kHz and a block of frequency dividers with division ratios 1 : 3, 1 : 5 and 1 : 10. With this clock, repetition periods within 1.25 ms to 62.5 s for a single channel can be obtained. The repetition period for the sequence of pulses from the three channels is three times greater than for a single channel because the repetition periods for the separate channels must be the same. Keying signals can also be delivered from the blocking oscillator in case a continuous adjustment of the repetition period is necessary. In that case, however, stability of the timer is lower than with the use of a quartz oscillator.

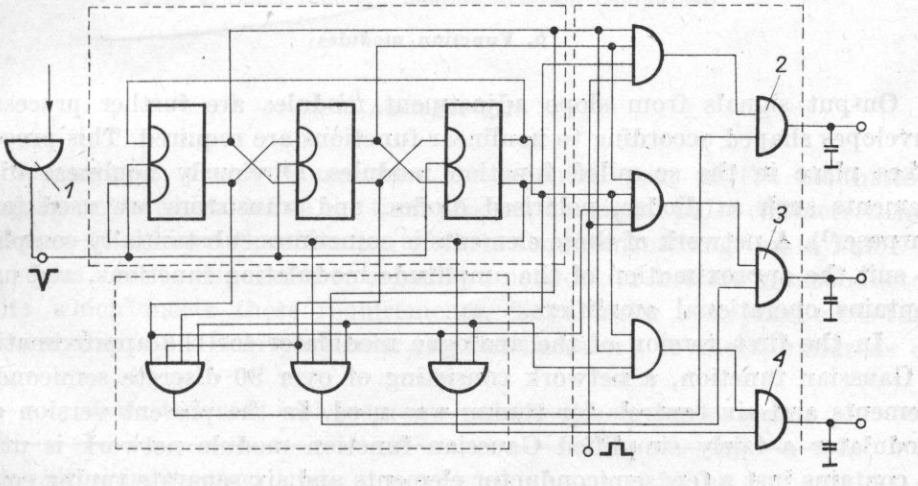

Fig. 2. Decoder logic diagram

1 — clock input, *2*, *3*, *4* — keying signal outputs for channel I, II and III

The order of operation of analogue gates is fixed with the use of a decoder which delivers consecutive pulses from the timer to the corresponding channels in an orderly fashion, i.e. each third pulse to the same channel. A block diagram of the decoder used is presented in Fig. 2. A conventional circuit terminated at both sides by additional NAND gates is used.

4. Duty time adjustment

Output pulses from the decoder are used in each channel to trigger the duty time adjustment circuit (that is, the keying pulse width adjustment circuit). These circuits are operating on a monoflop principle and have an externally adjustable time constant. In the first version of the modulator discrete elements were used in these circuits. In the present version integrated monoflops 74121 are used.

5. Slope adjustment

Time-locked keying pulses are then fed to the slope adjustment circuits. In these circuits the onset and cessation of a pulse are processed according to linear functions so that rise and decay times are adjustable within a range from 1 ms to 500 ms. Rise and decay times are equal (symmetrical envelope) and are externally adjustable in steps. Simple manipulation of internal helipots, however, will result in asymmetrical envelopes if required.

Slope adjustment modules are regarded as linear function modules if envelopes of the more sophisticated type are not required. In that case output signals from these modules are used directly to key analogue gates.

6. Function modules

Output signals from slope adjustment modules are further processed if envelopes shaped according to nonlinear functions are required. This processing takes place in the so-called function modules. Obviously nonlinear discrete elements such as diodes, polarised diodes, and transistors are used for this purpose(1). A network of these elements is sometimes substantially complicated to suit the approximation of the amplitude modulation functions, and usually contains operational amplifiers.

In the first version of the analogue modulator for the approximation of a Gaussian function, a network consisting of over 80 discrete semiconductor elements and six controls for tuning was used. In the present version of the modulator a fairly simplified Gaussian function module network is utilized. It contains just a few semiconductor elements and six separate tuning controls. The schematic diagram of this network is presented in Fig. 3(2). A similar network for the approximation of a sine function is presented in Fig. 4.

With careful tuning the accuracy of approximation is about 3% to 5% which is sufficient for research practice.

---

(1) Digital circuits are not taken into account for the sake of simplicity of modulator circuits.

(2) Patent applied for.

Monopolar keying signals thus obtained, which present time locked analogues of the definite functions, are further transformed to bipolar signals and are used for keying linear analogue gates.

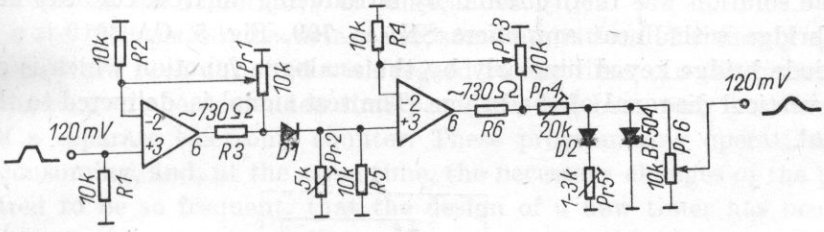

Fig. 3. Gaussian function module diagram (simplified)

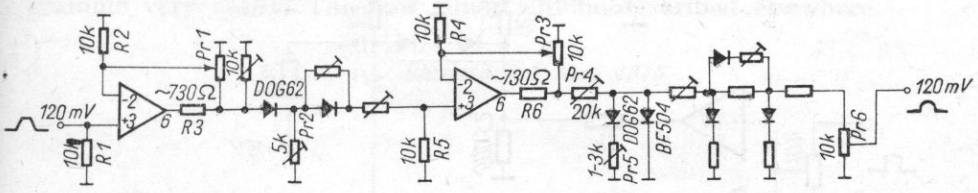

Fig. 4. Sin at function module diagram (simplified)

7. Analogue gate

Analogue gate clearly constitutes the essential part of the modulator. The requirements which define the final product i.e. signal pulse characteristics, are not easy to achieve. Specification of these requirements is given in Table 1.

It seems next to impossible to organize a network of discrete semiconductor elements which meets these requirements. To achieve a keying cross-talk level lower than 30 dB in particular, it was necessary to check hundreds of

Table 1. Linear analogue gate – specification of requirements

Test signal input-output level	2 V eff
Frequency band	0-20 kHz
Frequency response	±0,1 dB
Noise level with gate closed	−90 dB
Test signal cross-talk	−80 dB
Nonlinear distortion with gate opened	1%
Dynamic characteristics linearity	1%
Keying singal cross-talk	−50 dB
Keying voltage (monopolar)	100 mV
Operational times range	10^{-5}-10^{2} s

semiconductor elements to select just a few with close operating characteristics. The chances of arriving at sufficiently close characteristics are very thin indeed. 36 dB cross-talk of the keying signal was observed only in a constant ambient temperature with the use of extra resistor balance networks.

The solution was finally found by introducing an RCA CA 3019 integrated diode bridge with linear amplifiers SN μA 709, Fig. 5. CA 3019 is a resistive type diode bridge keyed bipolarly by the analogue function which is delivered to the vertical diagonal of the bridge. The test signal is delivered to the other diagonal.

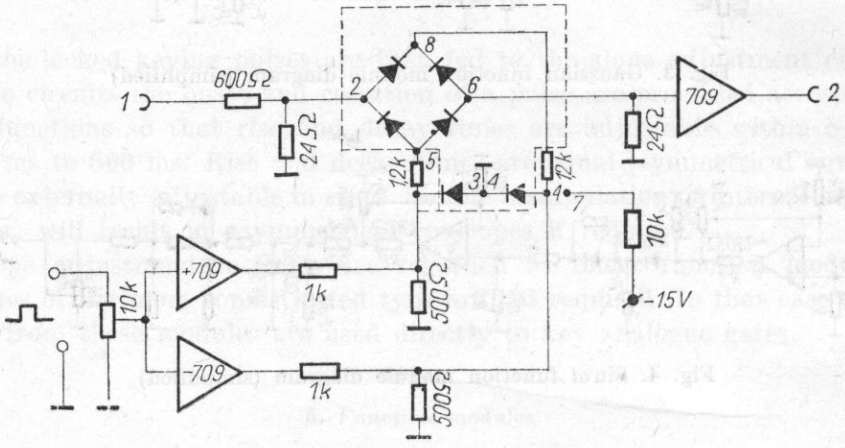

Fig. 5. Analogue gate module diagram (simplified)
1 – input, *2* – output

As all the diodes are on the same silica chip, their characteristics are fairly close, in fact much closer than it is possible to find in the discrete elements. To keep the keying cross talk at a level of – 50 dB, however, it is still necessary that the impedances at the test signal diagonal are low enough. In the present circuit this impedance should be 6 to 24 ohms. Also an accurate balance of the bipolar keying signals to 0.1% tolerance is needed.

To decrease nonlinear distortion of the test signal, its level should be low (of the order of few millivolts). Therefore amplification of the gate output to reach an overall gain of 0 dB, and an output level 2 V eff is necessary.

8. General remarks

It should be noted that for any chosen repetition period, the required duty time (or operational time) can be switched in by using duty time modules. In this way for repetition periods of the order of a few seconds, duty times can be of the order of 1 ms. Similarly it is possible that duty times overlap so that test signals are embedded in one another. To increase the possible range of

this overlapping, two duty time modules connected in series are introduced in one channel.

The described analogue modulator has been used for over two years in the research work concerning pitch perception in direct and residual masking carried out at the Laboratory of Musical Acoustics.

During that period of constant use, some limitations of a mainly operational character have been observed with regard to the timer. In the present version programming of the demanded time paradigm has been only possible with the use of a separate electronic counter. These programming operations were so time consuming, and, at the same time, the necessary changes of the paradigms appeared to be so frequent, that the design of a new timer has been decided upon.

The new timer is designed in TTL technique. It enables digital programming of the paradigms with a direct display and makes it possible to change the programme very easily. The new timer will be described elsewhere.

Received 3rd May 1975

C H R O N I C L E

XXIII OPEN SEMINAR ON ACOUSTICS
Jaszowiec, 6-11 September 1976

The Open Seminars on Acoustics have been organized in Poland since 1954 by the Polish Acoustical Society in cooperation with the Committee on Acoustics of the Polish Academy of Sciences. Each Seminar constitutes a review of the up-to-date results of investigations in all branches of acoustics followed in Poland. In recent years the number of participants has been approximately 300 including 10 to 20 participants from abroad. The proceedings of the Seminar are available during the conference and consist of the Polish text with the titles and abstracts in both Polish and English.

The XXIII Open Seminar in Jaszowiec will consist mainly of the contributed papers although a few invited papers will also be presented. The official language is Polish with simultaneous translation into English.

Address of the Organizing Committee: Chairman of Seminar, Dr A. Opilski, Politechnika Śląska, Gliwice, Polska.

1976 NOISE CONTROL CONFERENCE

The Conference is organized by the Committee on Acoustics of the Polish Academy of Sciences, in cooperation with the Polish Acoustical Society and the Institute of Fundamental Technological Research of the Polish Academy of Sciences. Assistance in organizing the technical program for the Conference is being provided by the Institute of Noise Control Engineering (INCE-USA).

Technical program:

1. Industrial noise
2. Transportation noise
3. Building noise
4. Community noise
5. Effects of noise and vibration on man
6. Methodology and instrumentation for noise and vibration measurement
7. Standards and legislation.

Three forms of presenting papers are planned: invited papers, contributed papers and poster-session papers.

For the poster-session, a meeting hall is filled with bulletin boards on which the lecturers place graphs, pictures, and a short text to illustrate the main points of their presentation. The authors will be expected to remain with their poster-display for some appointed

time to answer questions and discuss the paper with attendees. They will also be given 5 minutes' talk at the plenary session to introduce the main points of their work.

The conference language is English but there will be a translation into Polish.

Organizing Committee. Chairman of Conference: Prof. Stefan Czarnecki, Ph. D.; Secretary: Ewa Glińska (Mrs) M. Sc.

Address for correspondence: 76 Noise Control Conference, IPPT PAN, pokój 82, ul. Świętokrzyska 21, 00-049 Warszawa, Polska.

INTER-NOISE 77
Zurich, 1-3 March 1977

The INTER-NOISE 77 Conference is being organized by the Swiss Federal Institute of Technology (ETH) in Zurich. The conference is sponsored by the International Institute of Noise Control Engineering (INTERNATIONAL/INCE) in cooperation with other leading professional and government organizations.

Main themes:

1. NOISE CONTROL: the engineers' responsibility
2. Units, modern measurements and data acquisition methods
3. Noise prediction for land use planning and industrial environments
4. Optimum noise control in view of technical, economical and legal constraints

The topics of contributions should preferably relate to the main theme, however, contributed papers on any aspect of NOISE CONTROL ENGINEERING will also be considered for acceptance.

Schedule of paper preparation:

1 September 1976 – The deadline for the receipt of abstracts of about 500 words.

15 October 1976 – Notification of authors on the acceptance of their abstracts.

1 December 1976 – The deadline for receipt of manuscripts.

Abstracts and manuscripts should be written in English and should describe new material that has not been presented previously at a conference published in a journal.

Address of the Organizing Committee: Dr. Eric Rathe, Secretary General, International Institute of Noise Control Engineering, 8332 Zurich-Russikon, Switzerland.

9TH INTERNATIONAL CONGRESS ON ACOUSTICS
Madrid, 4-9 July 1977

The 9th International Congress on Acoustics will be organized by the Spanish Acoustical Society on behalf of the International Commission on Acoustics (ICA) of the International Union of Pure and Applied Physics (IUPAP).

The programme will comprise invited papers (30 minutes), contributed papers (15 minutes) and round table discussions.

Special emphasis will be given to the subject of ACOUSTICS and HABITAT: planning the acoustic environment. Classification of subjects:

I. Environmental acoustics

1. Acoustic criteria, 2. Design and planning, 3. Building acoustics, 4. Acoustic materials.

II. Noise and vibration

1. Noise sources, 2. Noise control, 3. Shock and vibration.

III. Psycho- and physiological acoustics

1. Hearing, 2. Speech and communication, 3. Bioacoustics.

IV. Physical acoustics

1. Ultrasound, 2. Underwater acoustics, 3. Molecular acoustics.

V. Electroacoustics

1. Sound systems, 2. Musical acoustics, 3. Instrumentation.

The deadline for receipt of the contributed papers, one page typed in official format is 1st December 1976.

In addition to the main Congress, two Satellite Symposia will be arranged:

Barcelona, 1-2 July 1977 – Sound recording and reproduction.

Sevilla, 11-12 July 1977 – Hearing and industrial noise environments.